

The Demography of Massive Dark Objects in Galaxy Centres

John Magorrian
Canadian Institute for Theoretical Astrophysics, University of Toronto,
60 St. George St., Toronto M5S 3H8, Canada
Electronic mail: magorrian@cita.utoronto.ca

Scott Tremaine
CIAR Cosmology and Gravity Program, Canadian Institute for Theoretical Astrophysics,
University of Toronto, 60 St. George St., Toronto M5S 3H8, Canada
Electronic mail: tremaine@cita.utoronto.ca

Douglas Richstone
Department of Astronomy, University of Michigan, Ann Arbor, MI 48109
Electronic mail: dor@astro.lsa.umich.edu

Ralf Bender
Universitäts-Sternwarte,
Scheinerstrasse 1,
München 81679, Germany
Electronic mail: bender@usm.uni-muenchen.de

Gary Bower
Kitt Peak National Observatory, National Optical Astronomy Observatories¹,
P.O. Box 26732, Tucson, AZ 85726
Electronic mail: gbower@noao.edu

Alan Dressler
The Observatories of the Carnegie Institution, 813 Santa Barbara St., Pasadena, CA 91101
Electronic mail: dressler@ociw.edu

S. M. Faber
UCO/Lick Observatory, Board of Studies in Astronomy and Astrophysics,
University of California, Santa Cruz, CA 95064
Electronic mail: faber@ucolick.org

Karl Gebhardt
Department of Astronomy, University of Michigan, Ann Arbor, MI 48109
Electronic mail: gebhardt@astro.lsa.umich.edu

Richard Green
Kitt Peak National Observatory, National Optical Astronomy Observatories¹,
P.O. Box 26732, Tucson, AZ 85726
Electronic mail: green@noao.edu

Carl Grillmair
Jet Propulsion Laboratory,
Mail Stop 183-900, 4800 Oak Grove Drive,
Pasadena, CA 91109
Electronic mail: carl@grandpa.jpl.nasa.gov

John Kormendy
Institute for Astronomy, University of Hawaii, 2680 Woodlawn Dr., Honolulu, HI 96822
Electronic mail: kormendy@oort.ifa.hawaii.edu

Tod R. Lauer
Kitt Peak National Observatory, National Optical Astronomy Observatories¹,
P.O. Box 26732, Tucson, AZ 85726
Electronic mail: lauer@noao.edu

¹ Operated by AURA under cooperative agreement with the U. S. National Science Foundation.

Abstract:

We construct dynamical models for a sample of 36 nearby galaxies with Hubble Space Telescope photometry and ground-based kinematics. The models assume that each galaxy is axisymmetric, with a two-integral distribution function, arbitrary inclination angle, a position-independent stellar mass-to-light ratio Υ , and a central massive dark object (MDO) of arbitrary mass M_\bullet . They provide acceptable fits to 32 of the galaxies for some value of M_\bullet and Υ ; the four galaxies that cannot be fit have kinematically decoupled cores. The mass-to-light ratios inferred for the 32 well-fit galaxies are consistent with the fundamental plane correlation $\Upsilon \propto L^{0.2}$, where L is galaxy luminosity. In all but six galaxies the models require at the 95% confidence level an MDO of mass $M_\bullet \sim 0.006M_{\text{bulge}} \equiv 0.006\Upsilon L$. Five of the six galaxies consistent with $M_\bullet = 0$ are also consistent with this correlation. The other (NGC 7332) has a much stronger upper limit on M_\bullet . We consider various parameterizations for the probability distribution describing the correlation of the masses of these MDOs with other galaxy properties. One of the best models can be summarized thus: a fraction $f \simeq 0.97$ of galaxies have MDOs, whose masses are well described by a Gaussian distribution in $\log(M_\bullet/M_{\text{bulge}})$ of mean -2.27 and width ~ 0.07 .

1 Introduction

The evidence that massive dark objects (MDOs) are present in the centers of nearby galaxies is reviewed by Kormendy & Richstone (1995; hereafter KR95). Further evidence that post-dates this review is described by Bender, Kormendy & Dehnen (1997), van der Marel et al. (1997) and Kormendy et al. (1997a). The MDOs are probably black holes, since star clusters of the required mass and size are difficult to construct and maintain, and since black-hole quasar remnants are expected to be common in galaxy centers; however, this identification is not important for the purposes of this paper. Following Kormendy (1993a), KR95 suggest that at least 20% of nearby hot galaxies (ellipticals and spiral bulges) have MDOs and point out that the observed MDO masses exhibit the correlation $M_\bullet \simeq 0.003M_{\text{bulge}}$, where M_{bulge} is the mass of the hot stellar component of the galaxy. (Throughout this paper we use the word “bulge” to refer to the hot stellar component of a galaxy, whether elliptical or spiral.) For a “bulge” with constant mass-to-light ratio Υ and luminosity L , $M_{\text{bulge}} \equiv \Upsilon L$.

The machinery for modelling the kinematics of hot galaxies to determine whether MDOs are present has increased steadily in sophistication over the past two decades. The earliest models (e.g. Young et al. 1978) fitted only the line-of-sight dispersion of spherical galaxies and assumed that the stellar distribution function was isotropic. Modern programs (e.g. Rix et al. 1997; Gebhardt et al. 1997) fit the entire line-of-sight velocity distribution for arbitrary axisymmetric galaxy models. While the most general and accurate possible models, and the highest resolution spectroscopic observations, were needed to establish the presence of the first few MDOs, we have learned with experience that estimates of the MDO mass based on cruder models and observations are usually fairly accurate. An example is the MDO in M87: Young et al. (1978) estimated the mass to be $\sim 5 \times 10^9 M_\odot$ from spherical, isotropic models, very close to the $3 \times 10^9 M_\odot$ determined by Harms et al. (1994) from HST spectra of a ring of ionized gas at 20 pc from the center.

This experience suggests that it is worthwhile to estimate MDO masses using relatively simple models applied to a large sample of galaxies. We cannot yet insist on HST spectroscopy for our sample, since this is still available only for a few galaxies; on the other hand HST photometry is available for over 60 hot galaxies. In this paper we examine a sample of 36 hot galaxies for which both HST photometry and reasonable quality, ground-based, long-slit spectroscopy are available. We look for evidence of MDOs among these by fitting two-integral axisymmetric dynamical models to the data for each galaxy. These are not the most general types of models, but they are quick to compute and will guide us towards galaxies to which we should apply more precise (and expensive) observations and models. Our results also provide a first look at the statistical distribution of MDOs as a function of galaxy luminosity and other parameters. They do *not*

establish unambiguously that an MDO is present in any individual galaxy.

The paper is organized as follows. The next section gives a brief outline of the data we use. This is followed by a detailed description of our modelling procedure and the assumptions that go in to it. Section 4 presents results for individual galaxies. What these tell us about the MDO mass distribution is tackled in Section 5. Finally Section 6 sums up.

2 Data

Our sample consists of all reasonably dust-free hot galaxies with HST photometry and ground-based velocity dispersion and rotation velocity profiles. The sample contains 36 galaxies, listed in Table 1 along with details of the sources of the observations we use. The Appendix contains comments about some of the galaxies. Most of the objects were observed prior to the first HST servicing mission with the Planetary Camera (0.043" per pixel) through filter F555W (roughly Johnson V). The sample includes galaxies observed in a number of HST programs (Lauer et al. 1992a,b, Grillmair et al. 1994, Jaffe et al. 1994, Forbes et al. 1995, Lauer et al. 1995); the reduction procedures are described by Lauer et al. (1995), Byun et al. (1996), and Faber et al. (1997). Some of the galaxies show evidence for nuclear activity. For each of these the table lists a radius R_{\min} , inside which non-stellar radiation probably makes a significant contribution to the observed light.

The HST data extend only to about 10" from the centre. For most of the galaxies we take published ground-based photometry and join it smoothly to the HST data to obtain a global photometric profile. For the remaining galaxies, we assume that the outer parts are well described by an $R^{1/4}$ profile with the same flattening as the outermost HST isophote. We take the effective radius of the $R^{1/4}$ profile from the literature, if available; otherwise we estimate it by fitting to the HST photometry.

Table 1 also lists the sources for our kinematical data. We restrict ourselves to reasonable quality CCD-based spectroscopy and do not use kinematical data beyond about two-thirds of the maximum radius for which photometry is available. Whenever there are many sources for a given slit position of a galaxy, we generally choose those with the best seeing. If an estimate for the seeing is unavailable we simply assume a FWHM of 2": the MDO masses yielded by our models are fairly insensitive to the precise value used, as long as it lies between 1" and 3".

The observations yield line-of-sight rotation speeds and velocity dispersions, convolved with seeing and averaged over spatial "bins" determined by the slit width and pixel size. We combine the measured rotation speed v_j and the velocity dispersion σ_j in each bin j to obtain an estimate of the second-order moment $\mu_j^2 = v_j^2 + \sigma_j^2$, which is the input used by our models. Strictly speaking, the v_j and σ_j quoted by observers do not individually have any direct connection with the moments of the line-of-sight velocity profiles (VPs), since they are usually obtained by fitting Gaussians to the VPs (van der Marel & Franx 1993). However, tests with flattened isotropic toy galaxies (Dehnen & Gerhard 1994; Magorrian & Binney 1994) show that there is typically an almost-constant difference of about 10% between the combination $v_j^2 + \sigma_j^2$ and the true second-order moments, with the sign of the difference changing from the major to the minor axis. Figure 1 shows a typical example. Since these differences are almost constant, they do not affect the MDO masses fitted by our models. They could, however, have a small effect on the fitted mass-to-light ratios.

Deriving the observational uncertainty $\Delta\mu_j$ is a vexing problem, because analysis methods used by different observers yield a range of error estimates Δv_j and $\Delta\sigma_j$, which usually do not take systematic effects, such as template mismatch, into account. We have tried the following three methods of dealing with this problem:

- (i) Simply take all quoted errors at face value;
- (ii) Replace Δv_j with $\max(\Delta v_j, 5 \text{ km s}^{-1})$ and similarly for $\Delta\sigma_j$;
- (iii) Scale the errors for each exposure along each slit position such that they are consistent with axisymmetry.

More precisely, suppose there are n measurements σ_j^+ along one side of a galaxy, with corresponding

measurements σ_j^- along the other side. We scale the $\Delta\sigma_j$ by a constant factor such that

$$\chi_\sigma^2 \equiv \sum_{j=1}^n \frac{(\sigma_j^+ - \sigma_j^-)^2}{(\Delta\sigma_j^+)^2 + (\Delta\sigma_j^-)^2} = n, \quad (1)$$

and similarly for the Δv_j (Davies & Birkinshaw 1988).

Notice that the last method implicitly assumes that the errors are Gaussian. This is almost certainly wrong, but it is the best we can do given the heterogeneous nature of our data. Given the ‘‘improved’’ observational errors, the error in μ_j is $\Delta\mu_j = (v_j^2(\Delta v_j)^2 + \sigma_j^2(\Delta\sigma_j)^2)^{1/2} / \mu_j$ to first order. We use (iii) above wherever possible, but the results of our models are usually not significantly affected by which procedure we employ.

3 Modelling Procedure

We assume that each galaxy is axisymmetric with some unknown inclination angle i , and work in cylindrical coordinates (R, ϕ, z) where the z -axis is the symmetry axis of the galaxy. A lower bound on i comes from requiring that all isophotes have an intrinsic axis ratio no less than 0.3 (i.e. no flatter than E7). Each galaxy can have a central MDO of arbitrary mass, but otherwise the mass-to-light ratio Υ is assumed to be independent of position. The distribution function of the stars is assumed to be a function only of two integrals of motion, the energy and the z -component of angular momentum. The advantage of these assumptions is that the (even part of the) kinematics follows uniquely from the three-dimensional luminosity distribution $\nu(R, z)$ (e.g., Lynden-Bell 1962; Dejonghe 1986). The disadvantage is that there is no reason why real galaxies should obey our assumptions. In particular, bright, core galaxies are usually non-rotating, and many studies of them (e.g., van der Marel 1991) show some evidence for radial anisotropy. Our two-integral models of flattened, non-rotating galaxies are *tangentially* anisotropic.

We use the modelling procedure introduced by Binney, Davies & Illingworth (1990) to predict the kinematics of each galaxy for any assumed inclination angle i and MDO mass M_\bullet . It predicts the second-order moments, convolved with seeing and averaged over the same $j = 1, \dots, n$ spatial bins used in the observations. The procedure is as follows:

1. Use a scheme based on maximum penalized likelihood to find a smooth luminosity density $\nu(R, z)$ that projects to an acceptable fit to the observed surface brightness (Magorrian 1997). The density ν is not uniquely determined by the surface brightness unless the galaxy is edge-on (Rybicki 1987). Romanowsky & Kochanek (1997) demonstrate that even for quite high inclinations there can be a large range in ν consistent with a given surface brightness; however, they find that the range of projected second-order moments associated with this uncertainty is quite small. We have carried out some experiments that confirm that the allowable MDO masses are not strongly affected by the indeterminacy in $\nu(R, z)$;
2. Calculate the gravitational potential and forces using an assumed stellar mass-to-light ratio Υ_0 and MDO mass M_\bullet ;
3. Use the Jeans equations to calculate the second-order moments $\overline{\nu v_\phi^2}$ and $\overline{\nu v_R^2} = \overline{\nu v_z^2}$;
4. Project the luminosity-weighted zeroth- and second-order moments of the line-of-sight velocity along the line of sight; convolve with seeing; and average over the same spatial bins used in the observations.

Dividing the binned, seeing-convolved second-order moment by the corresponding zeroth-order one yields the model’s predictions $\hat{\mu}_j^2(i, \Upsilon_0, M_\bullet)$ in each bin. These predictions scale trivially with mass-to-light ratio Υ through

$$\hat{\mu}_j^2(i, \Upsilon, M_\bullet) = \frac{\Upsilon}{\Upsilon_0} \hat{\mu}_j^2(i, \Upsilon_0, \Upsilon M_\bullet / \Upsilon_0). \quad (2)$$

3.1 Estimation of M_\bullet and Υ .

We assume that the measurement errors in the μ_j are Gaussian and uncorrelated. Then the likelihood of the photometric and kinematic data D given the model parameters (i, Υ, M_\bullet) is

$$p(D | i, \Upsilon, M_\bullet) \propto \exp\left(-\frac{1}{2}\chi^2\right), \quad (3)$$

where

$$\chi^2(i, \Upsilon, M_\bullet) \equiv \sum_{j=1}^n \left(\frac{\mu_j - \hat{\mu}_j}{\Delta\mu_j} \right)^2. \quad (4)$$

We obtain the best-fitting values M_\bullet and Υ and their confidence intervals as follows. By Bayes' theorem, the posterior distribution of i , Υ and M_\bullet given the data D is

$$p(i, \Upsilon, M_\bullet | D) \propto p(D | i, \Upsilon, M_\bullet) p(i | q') p(\Upsilon) p(M_\bullet), \quad (5)$$

where we have made the assumption that i , Υ and M_\bullet are *a priori* independent. Our priors $p(M_\bullet)$ and $p(\Upsilon)$ are flat in M_\bullet and $\log \Upsilon$ respectively. We make the reasonable assumption that the prior for i depends only on the observed axis ratio q' of the galaxy. Then $p(i | q')$ can be related to $N(q) dq$, the probability that a randomly chosen galaxy will have an intrinsic axis ratio lying between q and $q + dq$, by a further application of Bayes' theorem:

$$\begin{aligned} p(i | q') &= \frac{p(i) p(q' | i)}{p(q')} \\ &\propto p(i) \int p(q' | i, q) N(q) dq \\ &\propto \frac{1}{\sqrt{q'^2 - \cos^2 i}} N\left(\frac{(q'^2 - \cos^2 i)^{1/2}}{\sin i}\right), \end{aligned} \quad (6)$$

where we have made the natural assumption that $p(i) = \sin i$ and have used the relation $p(q' | i, q) \propto q' \delta(q^2 \sin^2 i + \cos^2 i - q'^2)$. We approximate the $N(q)$ obtained by Tremblay & Merritt (1995) by a Gaussian centred on $q = 0.7$ with standard deviation 0.1. Our results are only very weakly dependent on this form.

We are interested mainly in M_\bullet and Υ , not in i . Marginalizing the latter, we get the joint posterior distribution of Υ and M_\bullet as

$$p(\Upsilon, M_\bullet | D) = p(D | \Upsilon, M_\bullet) p(\Upsilon) p(M_\bullet), \quad (7)$$

where

$$p(D | \Upsilon, M_\bullet) \equiv \int p(D | i, \Upsilon, M_\bullet) p(i | q') di. \quad (8)$$

The posterior distributions $p(M_\bullet | D)$ and $p(\Upsilon | D)$ follow by marginalizing (7) again.

4 Results for individual galaxies

We have made models of each of our 36 galaxies for a range of $M_{\bullet} \geq 0$, Υ and i . The models do not provide adequate descriptions of the kinematics of four of the galaxies (NGC 1700, NGC 4365, NGC 4494 and NGC 4589). For these four, Figure 2(a) shows how χ^2 of equation (4) varies with MDO mass M_{\bullet} and inclination angle i . Figure 2(b) plots the kinematics of the models with the best-fitting values of M_{\bullet} against the observations. All four galaxies are known to have kinematically distinct cores (e.g., Forbes et al. 1996), so it is perhaps not surprising that our axisymmetric models do not work for them. We omit these four in the demographical analysis in the next section. For comparison, only two (NGC 3608 and NGC 4278) of the 32 galaxies that our models do fit are known to have kinematically distinct cores.

The models describe the kinematics of all of the remaining 32 galaxies reasonably well for some value of M_{\bullet} . Figure 3(a) shows the posterior distribution $p(\Upsilon, M_{\bullet} | D)$ in each case. Figure 3(b) shows the kinematics of the best-fitting models along each slit position fitted. Six of these galaxies have independent determinations of the mass of a central MDO. The comparison between the best-fit masses as determined here and the mass estimates in the literature for these six is presented in Figure 4. For all but one galaxy we obtain MDO masses that are in good agreement with those from earlier work. This gives us some degree of confidence in the assumptions that go into our models. The one exception is NGC 3115 for which Kormendy et al. (1996a) claim an MDO mass of about $2 \times 10^9 M_{\odot}$, some four times larger than our present mass estimate.

Our models imply that only three of the 32 galaxies (NGC 2778, NGC 4467, and NGC 7332) are consistent (at the 68% confidence level) with $M_{\bullet} = 0$. However, Figures 3(a) and (b) show that the available data for each of these three are also consistent with a reasonably large value of M_{\bullet} . NGC 7332 has the strongest upper limit on M_{\bullet} . In fact, the central dip in its dispersion profile is suggestive of either a mass-to-light ratio that decreases close to the centre, or else strong tangential anisotropy. Kormendy (1993b) has suggested that its formation history may be different from the other galaxies in the sample. We do not, however, omit it in the analysis below. There are a further three galaxies (NGC 4168, NGC 4473 and NGC 4636) consistent with $M_{\bullet} = 0$ at the 95% confidence level. All the rest have $M_{\bullet} > 0$.

Seven of the 32 galaxies show evidence for nuclear activity or strong dust obscuration. For these we make two types of models: one under the naïve assumption that all the observed light near the galaxy centre comes from stars, the other that only uses the photometry beyond a radius R_{\min} , where R_{\min} is given in Table 1. We find that the MDO masses predicted by the two types of models generally agree quite well. This is unsurprising given the relatively poor spatial resolution of the kinematical data. In what follows we use only the MDO masses obtained by omitting photometry within R_{\min} .

Table 2 lists the 68% confidence bounds that our models place on M_{\bullet} and Υ for the 32 galaxies. The correlations between Υ and L and between M_{\bullet} and M_{bulge} are plotted on Figure 5. Ignoring the error bars on Υ the formal best-fit straight line to $(\log L, \log \Upsilon)$ is

$$\log(\Upsilon_{\text{fit}}/\Upsilon_{\odot}) = (-1.12 \pm 0.33) + (0.18 \pm 0.03) \log(L/L_{\odot}) \quad (9)$$

with an RMS deviation between $\log \Upsilon_{\text{fit}}$ and $\log \Upsilon$ of 0.12. Our crude fit is broadly consistent with the fundamental-plane correlation $\Upsilon \propto L^{0.2}$ predicted using the virial theorem (e.g., Faber et al. 1987; Bender, Burstein & Faber 1992). Similarly, the correlation between M_{\bullet} and M_{bulge} for those galaxies with $M_{\bullet} > 0$ can be described by

$$\log(M_{\bullet,\text{fit}}/M_{\odot}) = (-1.82 \pm 1.36) + (0.96 \pm 0.12) \log(M_{\text{bulge}}/M_{\odot}), \quad (10)$$

with an RMS $(\log M_{\bullet,\text{fit}} - \log M_{\bullet})$ of 0.49. This result is consistent with the proportionality $M_{\bullet} \propto M_{\text{bulge}}$ that was first pointed out by Kormendy (1993a) and KR95. This apparent correlation is the subject of the next section.

Finally, we check whether there is any correlation between the residuals $x_i \equiv \log M_{\bullet,i} - \log M_{\bullet,\text{fit},i}$ and $y_i \equiv \log \Upsilon_i - \log \Upsilon_{\text{fit},i}$. One might expect a negative correlation if our models were fitting spuriously high MDO masses for some galaxies, thus depressing the fitted value of Υ . Figure 5(c) shows that there is no such correlation. The correlation coefficient $r_{xy} = 0.014$, which is not significant.

| | ω | $p_+(x \omega)$ |
|---------------------------------------|------------------------------|---|
| Power Law 1 – P_{PL1} | $(f, \log x_0, \alpha)$ | Nx^α if $x < x_0$; zero otherwise ($\alpha > -1$) |
| Power Law 2 – P_{PL2} | $(f, \log x_0, \alpha)$ | Nx^α if $x > x_0$; zero otherwise ($\alpha < -1$) |
| Schechter – P_{S} | $(f, \log x_0, \alpha)$ | $N(x/x_0)^\alpha \exp(-x/x_0)$ ($\alpha > -1$) |
| Gaussian – P_{G} | $(f, \log x_0, \log \Delta)$ | $N \exp[-\frac{1}{2}(x - x_0)^2/\Delta^2]$ |
| Log Gaussian – P_{LG} | $(f, \log x_0, \log \Delta)$ | $N \exp[-\frac{1}{2}(\log x - \log x_0)^2/\Delta^2]$ |

Table 3. The five parameterizations for $p(x | \omega)$ considered here. The variable $x \equiv M_\bullet/M_{\text{bulge}}$ where M_\bullet is the mass of the MDO and M_{bulge} is the mass of the hot stellar component of the galaxy. For a given set of parameters ω , the probability that a galaxy has an MDO with mass in the range $[x, x + dx]$ is $p(x | \omega, P) dx = (1 - f)\delta(x) dx + f p_+(x | \omega, P) dx$, where f is the fraction of galaxies with $M_\bullet > 0$ and the $N(\omega)$ in $p_+(x | \omega, P)$ is a normalizing factor (equation (12)). The prior probability $p(\omega | P)$ is assumed to be flat in the parameters ω .

5 MDO mass distribution

What do these new results tell us about the distribution of MDOs among galaxies? Let us assume initially that the MDO mass distribution of our sample depends only on $x \equiv M_\bullet/M_{\text{bulge}}$ and is characterized by some other parameters ω ; that is, that there is some function $p(x | \omega) dx$ which is the probability that a galaxy has an MDO with mass in the range $[x, x + dx]$.

We experiment with several parameterizations P for $p(x | \omega)$, as shown in Table 3. In each case, one of the parameters, f , is the fraction of galaxies with $M_\bullet > 0$, so that $p(x | \omega)$ is of the form

$$p(x | \omega, P) = (1 - f)\delta(x) + f p_+(x | \omega, P), \quad (11)$$

where $p_+(x | \omega, P)$ describes the distribution of MDOs with $M_\bullet > 0$. The $N(\omega)$ in $p_+(x | \omega, P)$ is a normalizing factor chosen such that

$$\int_0^\infty p_+(x | \omega, P) dx = 1. \quad (12)$$

The parameterizations P_{PL2} and P_{LG} assume that there is a genuine ridge line in $p(x)$ at $x = x_0$, whereas the other three also test whether KR95’s apparent ridge at $x \simeq 0.005$ is just the upper envelope of some ridgeless $p(x)$.

For each parameterization $P = (P_{\text{PL1}}, P_{\text{PL2}}, P_{\text{S}}, P_{\text{G}}, P_{\text{LG}})$, we first seek the most likely set of parameters ω given our data D . By Bayes’ theorem, the posterior distribution of ω and mass-to-light ratios $\Upsilon \equiv (\Upsilon_1, \dots, \Upsilon_N)$ of the 32 galaxies is

$$\begin{aligned} p(\omega \Upsilon | D, P) &\propto p(\omega | P) p(\Upsilon) p(D | \omega \Upsilon, P) \\ &\propto p(\omega | P) p(\Upsilon) \int p(D | \Upsilon \mathbf{x}) p(\mathbf{x} | \omega, P) d\mathbf{x}, \end{aligned} \quad (13)$$

where $p(D | \Upsilon \mathbf{x})$ is a product of factors of the form of equation (8). The prior $p(\omega | P)$ is assumed flat in the parameters ω given in Table 3. We are interested only in the parameters ω , not in Υ . Marginalizing the latter yields

$$\begin{aligned} p(\omega | D, P) &= \int p(\omega \Upsilon | D, P) d\Upsilon \\ &\propto p(\omega | P) \int p(D | \mathbf{x}) p(\mathbf{x} | \omega, P) d\mathbf{x}, \\ &\propto p(\omega | P) \prod_{j=1}^N \int p(D_j | x_j) p(x_j | \omega, P) dx_j, \end{aligned} \quad (14)$$

where we have defined

$$p(D | \mathbf{x}) \equiv \int p(D | \Upsilon \mathbf{x}) p(\Upsilon) d\Upsilon, \quad (15)$$

and similarly for $p(D_j | x_j)$.

The posterior distributions $p(\omega | D, P)$ for each parameterization are plotted on Figure 6. Table 4 lists the best-fitting parameters with their 68% confidence intervals and Figure 7 plots $p(x | \omega, P)$ for the best-fitting parameters ω in each case. According to all parameterizations except P_{PL1} , nearly all galaxies have MDOs ($f \simeq 0.96$) with means $\langle x \rangle \simeq 0.01$ and $\langle \log x \rangle \simeq -2.25$, consistent with the KR95 interpretation. However, the best-fitting parameters from both P_{PL2} and P_{LG} imply that there is a genuine ridge in $p(x)$ at this mean x , whereas both P_{PL1} and P_{S} say there is *no* ridge, since they prefer $\alpha < 0$. The Gaussian parameterization P_{G} is inconclusive: there is not a strong lower limit on x_0 in this case, since the most likely value of the other parameter Δ is comparable in size to x_0 .

Which of the five parameterizations gives the better description of the real $p(x)$? Using Bayes' theorem again, the plausibility of the parameterization P given the available data D is

$$\begin{aligned} p(P | D) &= \frac{p(P)p(D | P)}{p(D)} \\ &= \frac{p(P)}{p(D)} \int p(D | \omega, P) p(\omega | P) d\omega. \end{aligned} \quad (16)$$

If we assume that all of the parameterizations are *a priori* equally likely, i.e., $p(P_{\text{PL1}}) = p(P_{\text{PL2}}) = p(P_{\text{S}}) = p(P_{\text{G}}) = p(P_{\text{LG}})$, then we find that $p(P_{\text{PL2}} | D) = 4.0 p(P_{\text{LG}} | D) \simeq 2 \times 10^5 p(P_{\text{S}} | D) \simeq 10^{10} p(P_{\text{PL1}} | D) \simeq 7 \times 10^{10} p(P_{\text{G}} | D)$: P_{PL2} and P_{LG} provide by far the best description of the five. This result suggests that there really is a ridge in $p(x)$ at $\log x \simeq -2.2$.

It is also instructive to try to obtain a “non-parametric” estimate of $p(x)$. We take n parameters $\omega_1 \dots \omega_n$ with $n = 50$. We define ω_i as the probability that a randomly chosen galaxy has an MDO whose mass lies between x_{i-1} and x_i , where x_i runs logarithmically from $x_1 = 10^{-5}$ to $x_{50} = 1$, and $x_0 = 0$. A reasonable prior guess for $p(x)$ (and therefore the ω_i) is a power law. So we choose

$$\log p(\omega) = -\frac{\lambda}{n} \sum_{i=2}^{n-1} \left(\frac{\log \omega_{i+1} - 2 \log \omega_i + \log \omega_{i-1}}{(\Delta \log x)} \right)^2, \quad (17)$$

where the free parameter λ controls how smooth (i.e., how far from a pure power law) we think an acceptable $p(x)$ ought to be. We use 10^6 iterations of the Metropolis algorithm (Metropolis et al. 1953; see also Saha & Williams 1994) to obtain the posterior distribution $p(\omega | D)$ for each ω_i for a range of λ . The results for $\lambda = 5$ are plotted on Figure 7(b). The “non-parametric” distributions $p(x)$ calculated in this way are broadly the same as the those obtained from the best parameterizations P_{PL2} and P_{LG} .

Thus far we have assumed that the MDO mass distribution depends only on $x \equiv M_{\bullet}/M_{\text{bulge}}$, but there is no good reason for assuming that M_{\bullet} should be correlated with the mass rather than, say, the luminosity of the bulge. Consider a more general form,

$$x' \equiv \left(\frac{M_{\bullet}}{M_{\odot}} \right) \left(\frac{L_{\odot}}{L} \right) \left(\frac{\Upsilon_{\odot}}{\Upsilon} \right)^a, \quad (18)$$

where a is a free parameter. The analysis above can be carried out with x replaced by x' . Setting $a = 1$ tests the correlation of M_{\bullet} with M_{bulge} (the case we have just considered), whereas setting $a = 0$ tests its correlation with L . The results of our calculations of $p(P | D, a)$ for a range of a are plotted on Figure 8. Clearly, the case $a = 1$ is the most plausible – M_{\bullet} is much more strongly correlated with the mass of the bulge than the luminosity.

Finally, a simple confirmation of the proportionality between M_{\bullet} and M_{bulge} can be obtained by splitting the sample of 32 galaxies into the most luminous half and the least luminous half, and then calculating $p(\omega | D, P)$ for each subsample for each parameterization. With the exception of the poorly fitting parameterization P_{PL1} , we find that the best-fitting parameters ω calculated using each subsample lie within the 95% confidence region of the parameters calculated using the full sample.

6 Conclusions

We have examined a sample of 36 galaxy bulges and found that the kinematics of 32 of them are described well by two-integral axisymmetric models. Among these 32, a substantial MDO is required in all but four in order for our models to reproduce the observed kinematics. We have considered a range of models for the demography of these MDOs. In the best-fitting models about 96% of galaxies have an MDO. The mass of this MDO is strongly correlated with the bulge mass, with an MDO-to-bulge mass ratio of around 0.005. Possible explanations for this correlation have already been discussed by Faber et al. (1997). The galaxies without MDOs perhaps have a different formation history; one possible scenario has been put forward by Kormendy (1993b).

The mass-to-light ratios Υ fit by our models scale with luminosity L as $\Upsilon \propto L^{0.2}$, which is just the usual fundamental plane correlation. Since our models take full account of the shape of the light distribution of each galaxy, they rule out any attempts to explain the slope of the fundamental plane by a “non-homology” of the light profiles (e.g., Graham & Colless 1997, and references therein). Our models do not, however, consider the possibility of a systematic change in orbital anisotropy with luminosity (Ciotti et al. 1996).

These results are based on an “assembly-line” approach to building galaxy models, which is necessarily less accurate than building models for each galaxy by hand. In particular:

- (i) Some or all of the galaxies may not be axisymmetric.
- (ii) Even if the galaxies are axisymmetric, our two-integral models are not the most general possible. For some or all of the galaxies, there may exist more general three-integral models that can reproduce the observed kinematics (and, indeed, the full line-of-sight velocity profiles) without needing to invoke MDOs – see Kormendy et al. (1997a) for an example.
- (iii) The selection criteria used to derive this sample are heterogeneous and impossible to quantify, although any biases introduced by properties such as luminosity, core size, and surface brightness are accounted for by the analysis procedure in §3.
- (iv) The assumption that the mass-to-light ratio is independent of position outside the centre may not be correct.

Of the points above, the most important is perhaps (ii) – our conclusions are most uncertain due to our assumption of a two-integral distribution function. We should know soon whether more general three-integral models (e.g., Rix et al. 1997, Gebhardt et al. 1997, Richstone et al. 1997) will relax the need for MDOs in at least some of the galaxies in our sample. However, it is not yet clear what mechanism could effect just the right degree of radial anisotropy in each galaxy to cause the apparent correlation $M_{\bullet} \propto M_{\text{bulge}}$ as seen by our two-integral models.

Acknowledgements: We thank Jesús González for providing kinematical data from his thesis. Our collaboration was supported by HST data analysis funds through GO grants GO-2600.01.87A and GO-06099.01-94A, by NASA grant NAS-5-1661 to the WFPC1 IDT, and by grants from NSERC. ST acknowledges support from an Imasco fellowship. We thank the Fields Institute for Research in Mathematical Sciences at the University of Toronto and OCIW for their hospitality during part of this work.

References

- Bender R., Döbereiner S., Möllenhoff C., 1987 *A&A*, 177, 53 (BDM)
- Bender R., Nieto J.-L., 1990, *A&A*, 239, 97 (BN)
- Bender R., Burstein D., Faber S.M., 1992, *ApJ*, 399, 462
- Bender R., Saglia R.P., Gerhard O.E., 1994, *MNRAS*, 269, 785 (BSG)
- Bender R., Kormendy J., Dehnen W., 1996, *ApJ*, 464, L119 (BKD)
- Binney J.J., Davies R.L., Illingworth G.D., 1990, *ApJ*, 361, 78 (BDI)
- Byun Y.I., et al., 1996, *AJ*, 111, 1889
- Ciotti L., Lanzoni B., Renzini A., 1996, *MNRAS*, 282, 1
- Davies R., Birkinshaw M., 1988, *ApJS*, 68, 409 (DB)
- Dehnen W., Gerhard O.E., 1994, *MNRAS*, 268, 1019
- Dejonghe H., 1986, *Phys. Rep.*, 133, 218
- Faber S.M., Dressler A., Davies R.L., Burstein D., Lynden-Bell D., Terlevich R., Wegner G., 1987, in “Nearly Normal Galaxies, From the Planck Time to the Present”, ed. S.M. Faber (NY: Springer), 317
- Faber S.M., et al., 1997, preprint
- Fisher D., Illingworth G., Franx M., 1994, *AJ*, 107, 160 (FIF94)
- Fisher D., Illingworth G., Franx M., 1995, *ApJ*, 438, 539 (FIF95)
- Forbes D. A., Franx M., & Illingworth G. D. 1995, *AJ*, 109, 1988
- Forbes D.A., Franx M., Illingworth D., Carollo C.M., 1996, *ApJ*, 467, 126
- Franx M., Illingworth G., Heckman T., 1989, *ApJ*, 344, 613 (FIH)
- Gebhardt K., Richstone D., et al., 1997, (G97) (n3379)
- González J., 1993, Ph.D. thesis, UC Santa Cruz (G93)
- Graham A., Colless M.M., submitted to *MNRAS* (astro-ph/9701020)
- Grillmair C.J., et al. 1994, *AJ*, 108, 102
- Harms R.J., et al., 1994, *ApJ*, 435, L35
- Jaffe W., 1983, *MNRAS*, 202, 995
- Jaffe W., et al., 1994, *AJ*, 108, 1567
- Jedrzejewski R., Schechter P.L., 1989, *AJ*, 98, 147 (JS)
- Kent S.M., 1987, *AJ*, 94, 306 (Ke87)
- Kormendy J., 1988, *ApJ*, 335, 40 (K88) (n4594)
- Kormendy J., 1993a, in “The Nearest Active Galaxies”, ed. J. Beckman, L. Colina & H. Netzer (Madrid: Consejo Superior de Investigaciones Cientificas), p. 197
- Kormendy J., 1993b, in *IAU Symposium 153*, “Galactic Bulges”, eds. H. Habing and H. Dejonghe, Kluwer: Dordrecht
- Kormendy J., Richstone D., 1992, *ApJ*, 393, 559 (KR92)
- Kormendy J., Richstone D., 1995, *ARA&A*, 33, 581 (KR95)
- Kormendy J., et al., 1996a, *ApJ*, 459, L57 (K96a) (n3115)
- Kormendy J., et al., 1996b, *ApJ*, 473, L91 (K96b) (n4594)
- Kormendy J., et al., 1997a, *ApJ*, 482, L139 (K97a) (n4486b)
- Kormendy J., et al., 1997b, preprint (K97b) (n3377).
- Kormendy J., Bender R., 1997, preprint (KB97)
- Lauer T.R., et al., 1992a, *AJ*, 103, 703 (L92a) (M87)
- Lauer T.R., et al., 1992b, *AJ*, 104, 552 (L92b) (M32)
- Lauer T.R., et al., 1993, *AJ*, 106, 1436
- Lauer T.R., et al. 1995, *AJ*, 110, 2622
- Lynden-Bell D., 1962, *MNRAS*, 123, 447
- Magorrian S.J., 1997, in preparation
- Magorrian S.J., Binney J.J., 1994, *MNRAS*, 271, 949
- Metropolis N., et al., 1953, *J. Chem. Phys.*, 21, 1087
- Peletier R.F., Davies R.L., Illingworth G.D., Davis L.E., Cawson M., 1990, *AJ*, 100, 1091 (PDIDC)
- Richstone D., Bower G., Dressler A., 1990, *ApJ*, 353, 118
- Richstone D., et al., 1997, in preparation

Rix H.W., de Zeeuw P.T., Carollo C.M., Cretton N., van der Marel R.P., 1997, preprint
Romanowsky A. J., & Kochanek C. S., 1997, MNRAS, 287, 35
Rybicki G., 1987, in Structure and Dynamics of Elliptical Galaxies, ed. T. de Zeeuw (Dordrecht: Kluwer), 397.
Saha P., Williams T.B., 1994, AJ, 107, 1295
Scorza C., Bender R., 1995, AJ, 293, 20 (SB)
Tremaine S., 1995, AJ, 110, 628
Tremblay B., Merritt D., 1995, AJ, 110, 1039
van der Marel R.P., 1991, MNRAS, 253, 710
van der Marel R.P., 1994, MNRAS, 270, 271 (vdM94a) (M87)
van der Marel R.P., Franx M., 1993, ApJ, 407, 525
van der Marel R.P., Rix H.-W., Carter D., Franx M., White S.D.M., de Zeeuw T., 1994, MNRAS, 268, 521 (vdM94b)
(M31,M32,n3115,n4594)
van der Marel R.P., de Zeeuw P., Rix H.-W., Quinlan G.D., 1997, Nature 385, 610
Young P., Westphal J.A., Kristian J., Wilson C.P., Landauer F.P., 1978, ApJ, 221, 721

A Appendix: Notes on individual galaxies

M31: This galaxy has a double nucleus (e.g., Lauer et al. 1993), but axisymmetric models should still provide a reasonable description of the gross features of its kinematics. We use kinematical data from van der Marel et al. (1994) and Kormendy & Bender (1997). The former appear to measure major-axis radii from the photometric centre of the galaxy, rather than the kinematic centre, which we assume to be coincident with the fainter nucleus (e.g., Tremaine 1995). Thus we add 0.3 arcsec to van der Marel et al.'s quoted major-axis positions. We do not fit to kinematical data beyond 10 arcsec because the outer photometry we use (Kent 1987) consists only of a major- and a minor-axis profile with no additional isophote shape information.

NGC 1600: Both Jedrzejewski & Schechter (1989) and Bender, Saglia & Gerhard (1994) give major- and minor-axis kinematics for this galaxy. There are many more outlier points in the latter data, so we reject it.

NGC 2778: Fisher, Illingworth & Franx (1995; FIF95) and González (1993; G93) give major-axis profiles. Both G93 and Jedrzejewski & Schechter (1989) give minor axis profiles. FIF95's central dispersion is inconsistent with the others, so we reject their data for this galaxy.

NGC 3379: The best kinematical data comes from Gebhardt et al. (1997). We restrict our model fits to their ground-based data within 12 arcsec of the centre.

NGC 4486: We use the blue G-band kinematics from van der Marel (1994), and reject his infrared kinematics which are probably affected by template mismatch. In the same paper, van der Marel presents evidence that this galaxy is radially anisotropic in its outer parts. Therefore we restrict our model fits to the kinematics within the innermost 5 arcsec.

NGC 4594: The ground-based outer photometry (Kormendy 1988) consists only of a major- and a minor-axis profile. Because of this, and because of the problems with dust obscuration, we only use kinematical data within 8 arcsec.

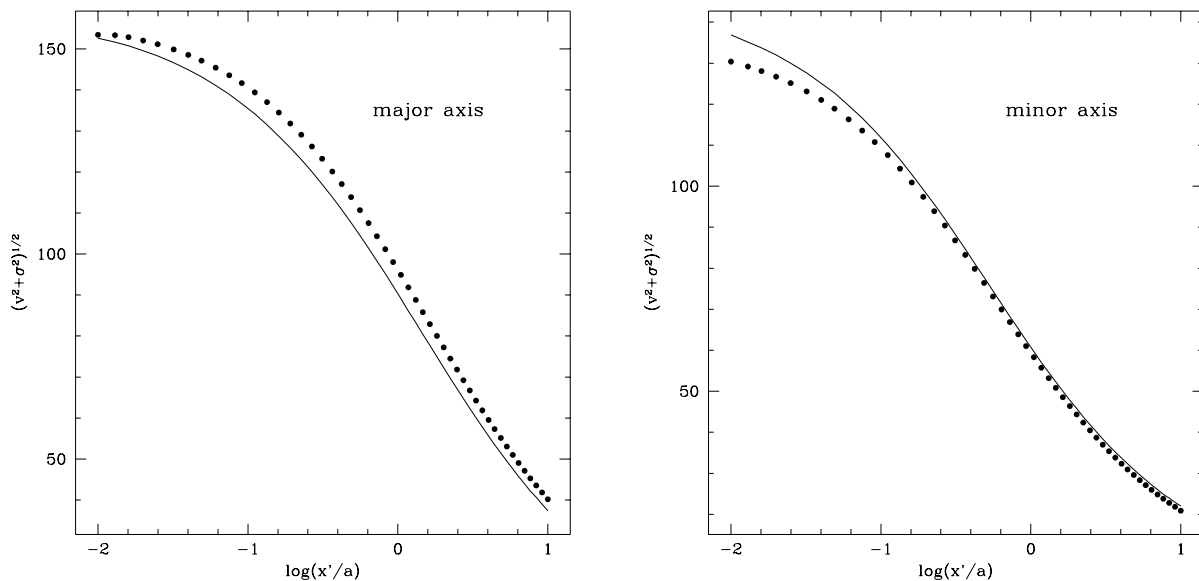


Figure 1. Major- and minor-axis projected second-moment profiles for a flattened (axis ratio $q = 0.6$) isotropic (rotating) Jaffe (1983) model viewed edge on. The curves show the (square root of the) classical second-order moments. The points plot the approximation $(v^2 + \sigma^2)^{1/2}$ where v and σ are the parameters of the best-fitting Gaussians to the line-of-sight velocity profiles.

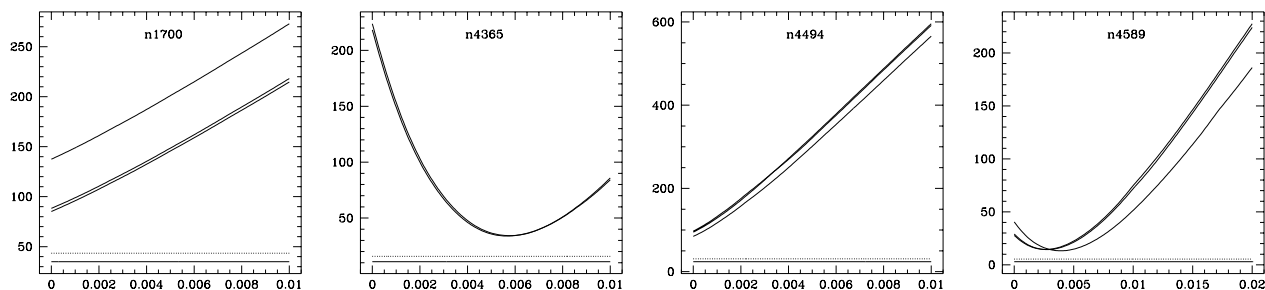


Figure 2(a). Plots of χ^2 versus M_*/M_{bulge} for the four galaxies that our models do not describe well. The different curves on each plot correspond to different assumed inclinations. A reasonable fit would have $\chi^2 \approx N_{\text{dof}} \pm (2N_{\text{dof}})^{1/2}$ where the number of degrees of freedom, N_{dof} , is related to n , the number of kinematical bins used in the fit, by $N_{\text{dof}} = n - 2$. The heavy solid and dashed lines show $\chi^2 = N_{\text{dof}}$ and $\chi^2 = N_{\text{dof}} + (2N_{\text{dof}})^{1/2}$ respectively.

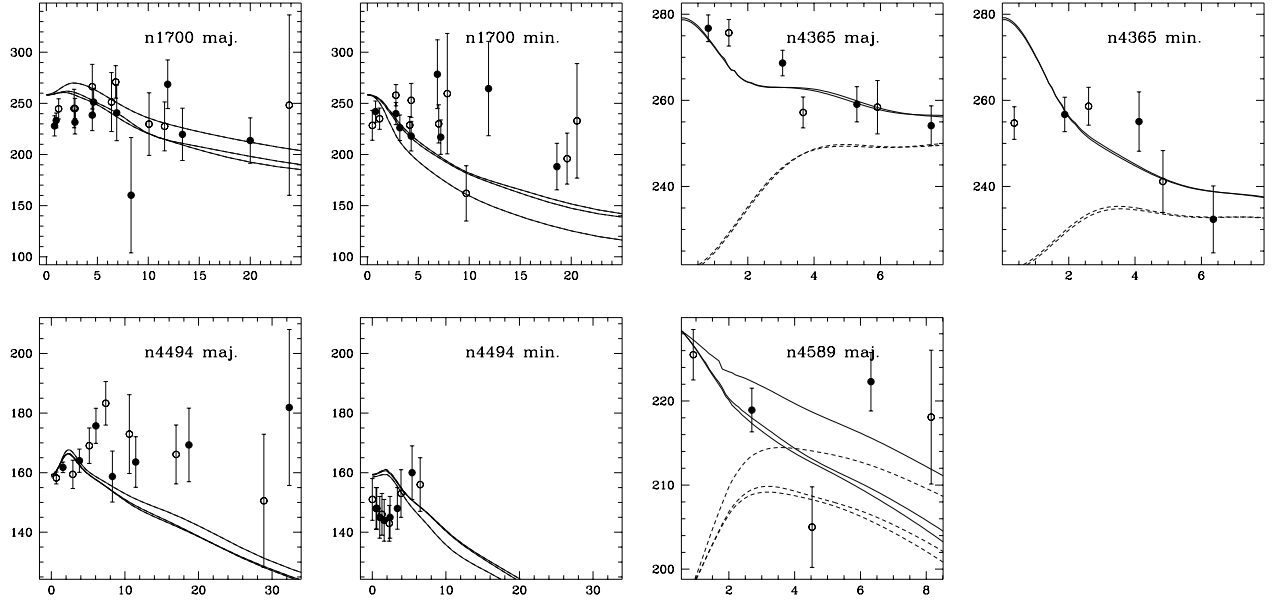


Figure 2(b). Kinematical profiles of the best-fitting models along each slit position used for the galaxies in Figure 2(a). The plots show $(v^2 + \sigma^2)^{1/2}$ (in units of km s^{-1}) versus distance from the centre of the galaxy (in arcsec). The observed kinematics are plotted as circles, open or closed depending on which side of the galaxy the observation was made. The solid curves show the model predictions (convolved with the same seeing as the best ground-based observations) for the best-fitting value of M_\bullet and Υ for each galaxy. The results for each assumed inclination angle are plotted as separate curves. For comparison the dashed curves plot the model predictions with the same value of Υ as above but $M_\bullet = 0$.

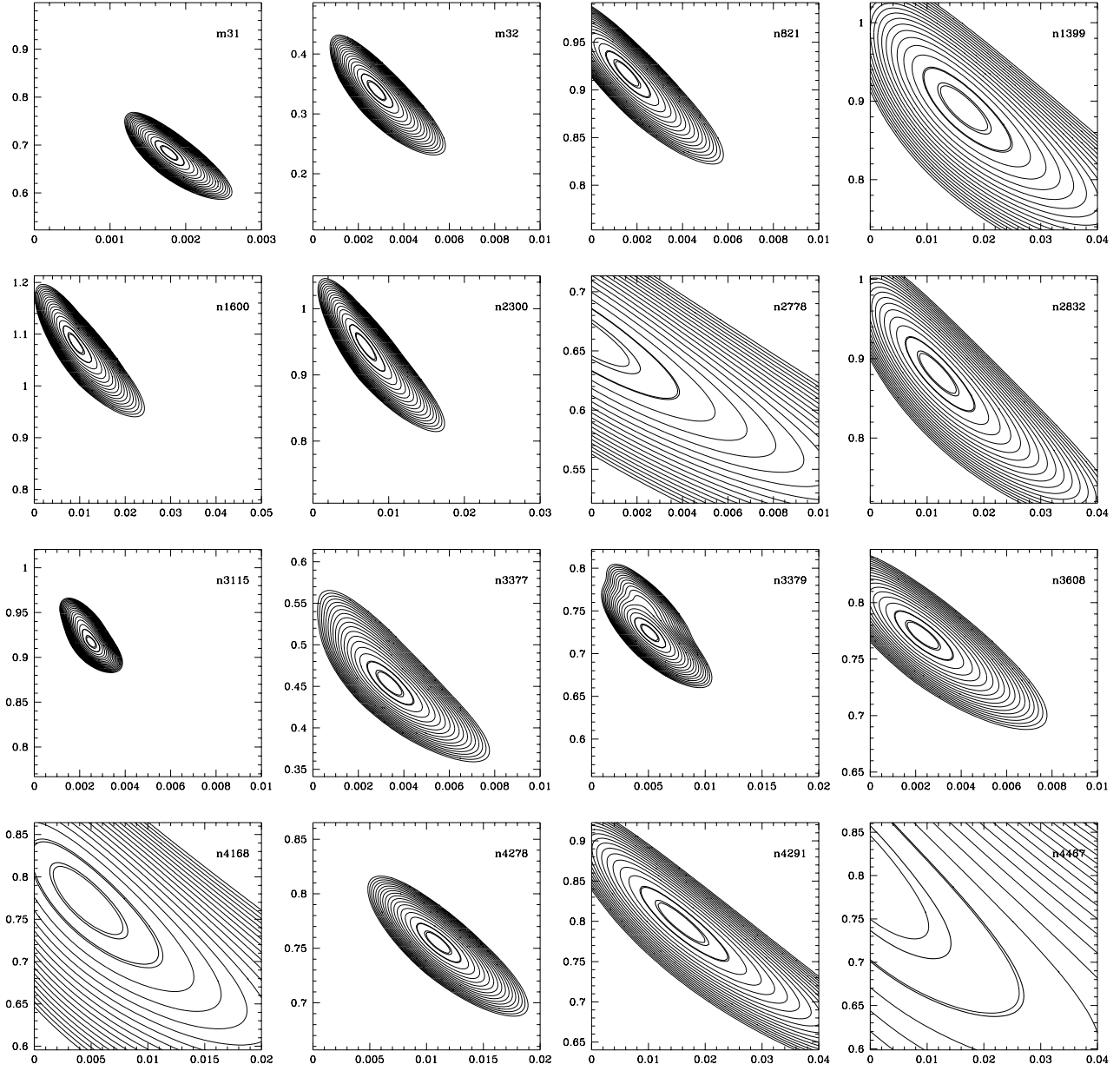


Figure 3(a). The posterior distributions $p(\Upsilon, M_{\bullet} \mid D)$ for all 32 galaxies that our models describe well. The vertical and horizontal axes are $\log(\Upsilon/\Upsilon_{\odot})$ and $M_{\bullet}/M_{\text{bulge}}$ respectively. Successive light contours indicate a factor of ten change in $p(\Upsilon, M_{\bullet} \mid D)$. The heavy contours enclose the 68% and 95% confidence regions on Υ and M_{\bullet} .

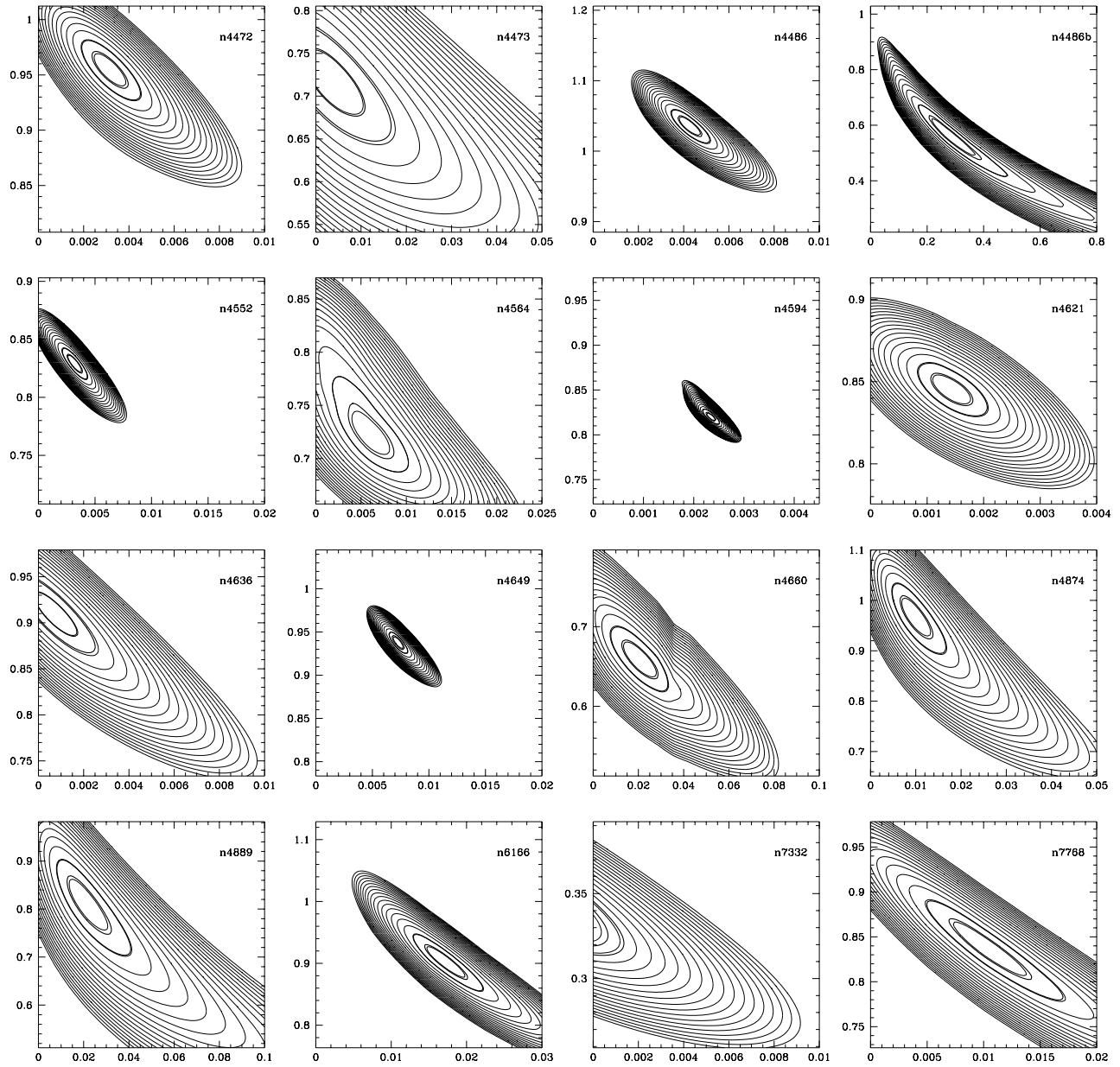


Figure 3(a)...continued.

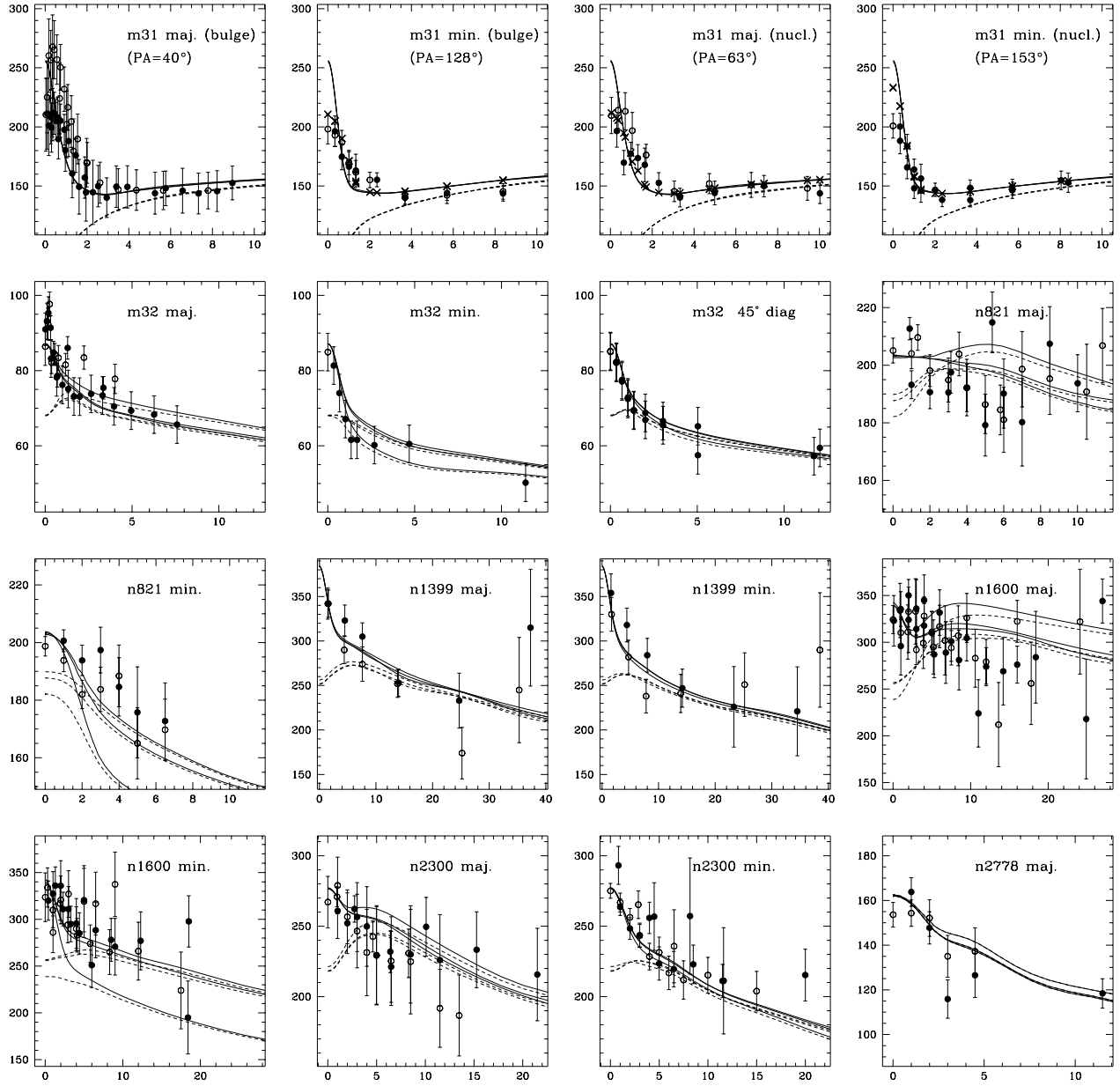


Figure 3(b). As for Figure 2(b), but for the galaxies that our models describe well. We also plot crosses to show the *spatially binned*, seeing-convolved model predictions for those cases where this quantity differs significantly from the unbinned model predictions (described by the curves).

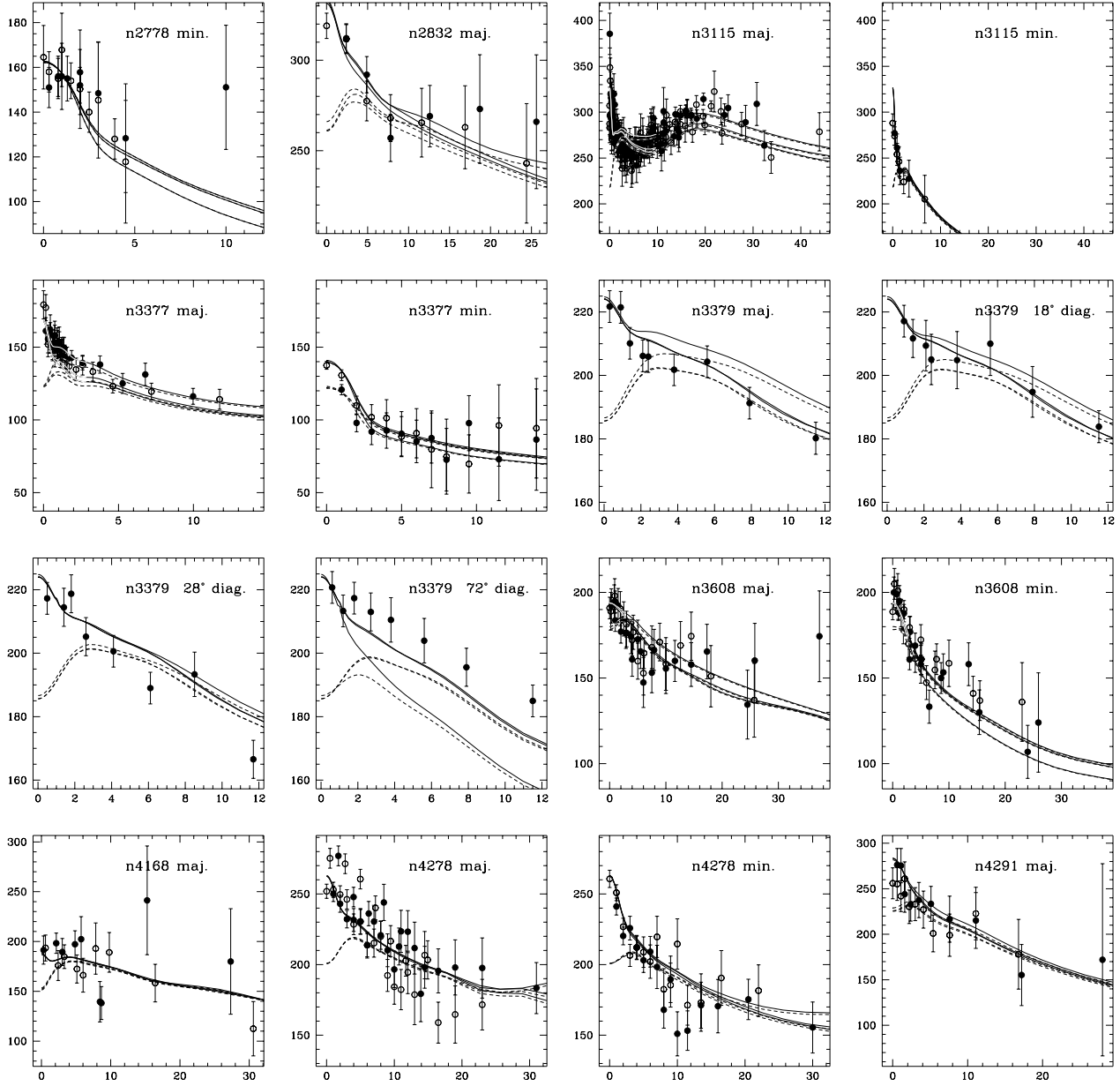


Figure 3(b)...continued.

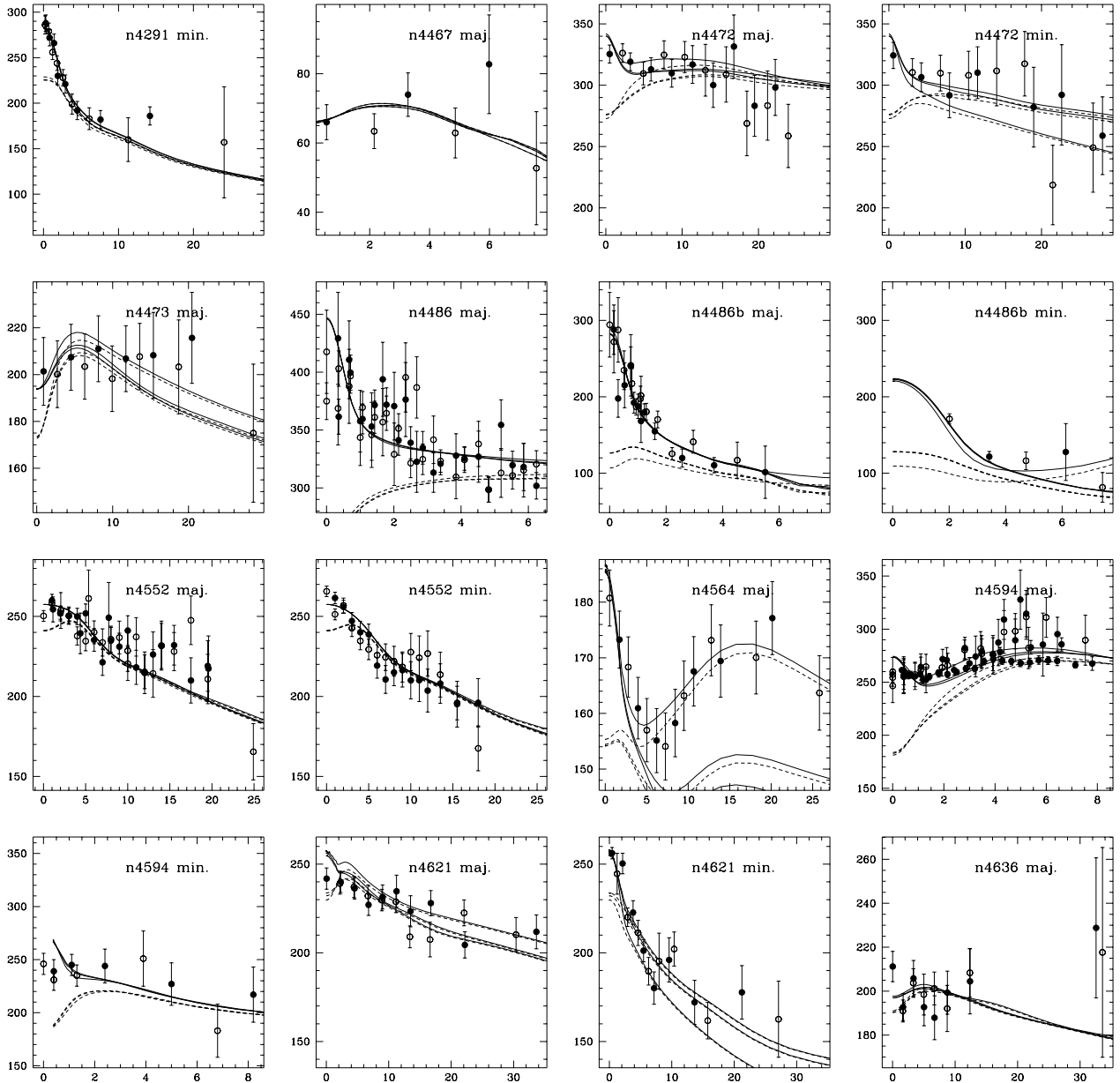


Figure 3(b)...continued.

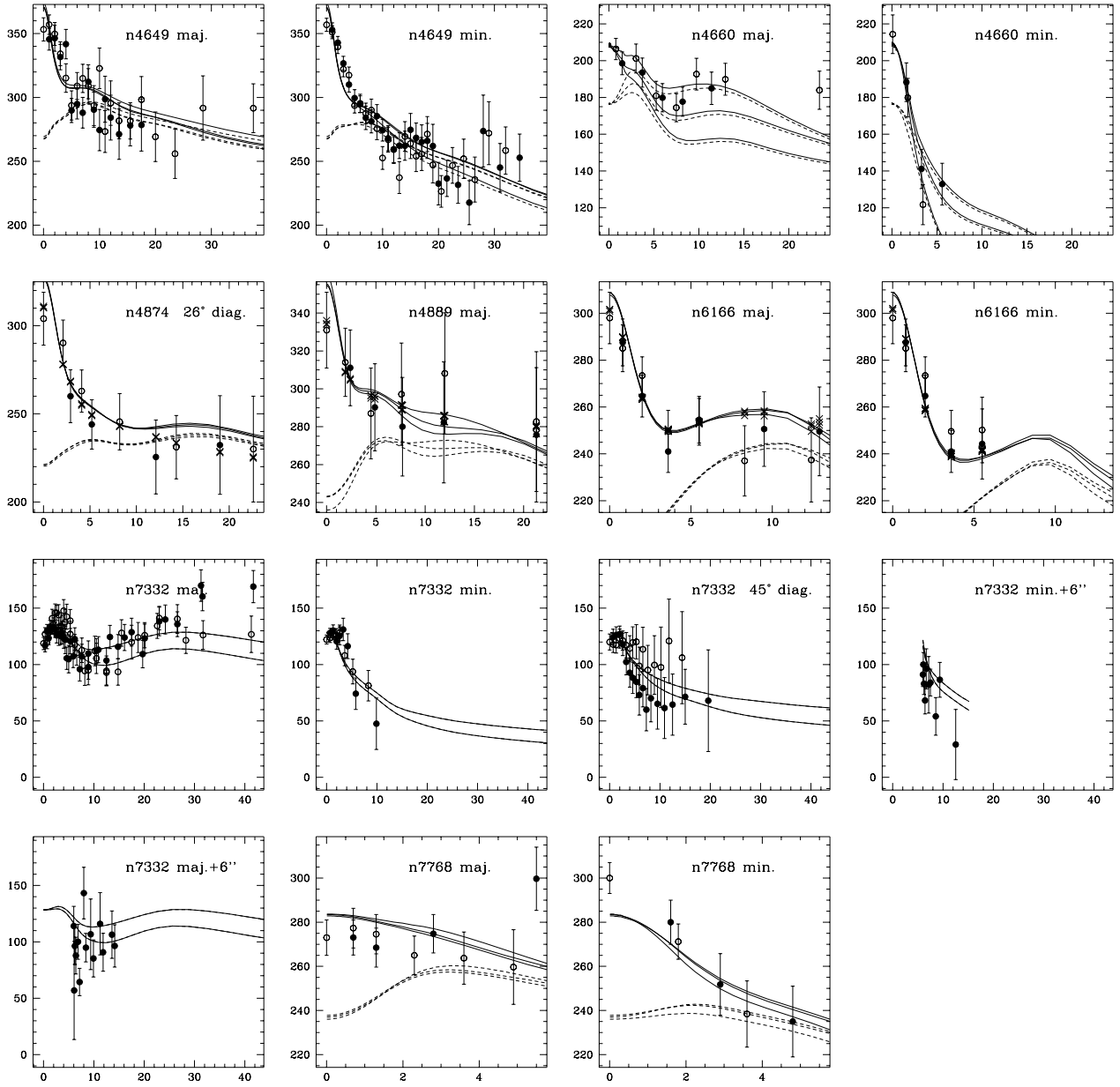


Figure 3(b)...continued.

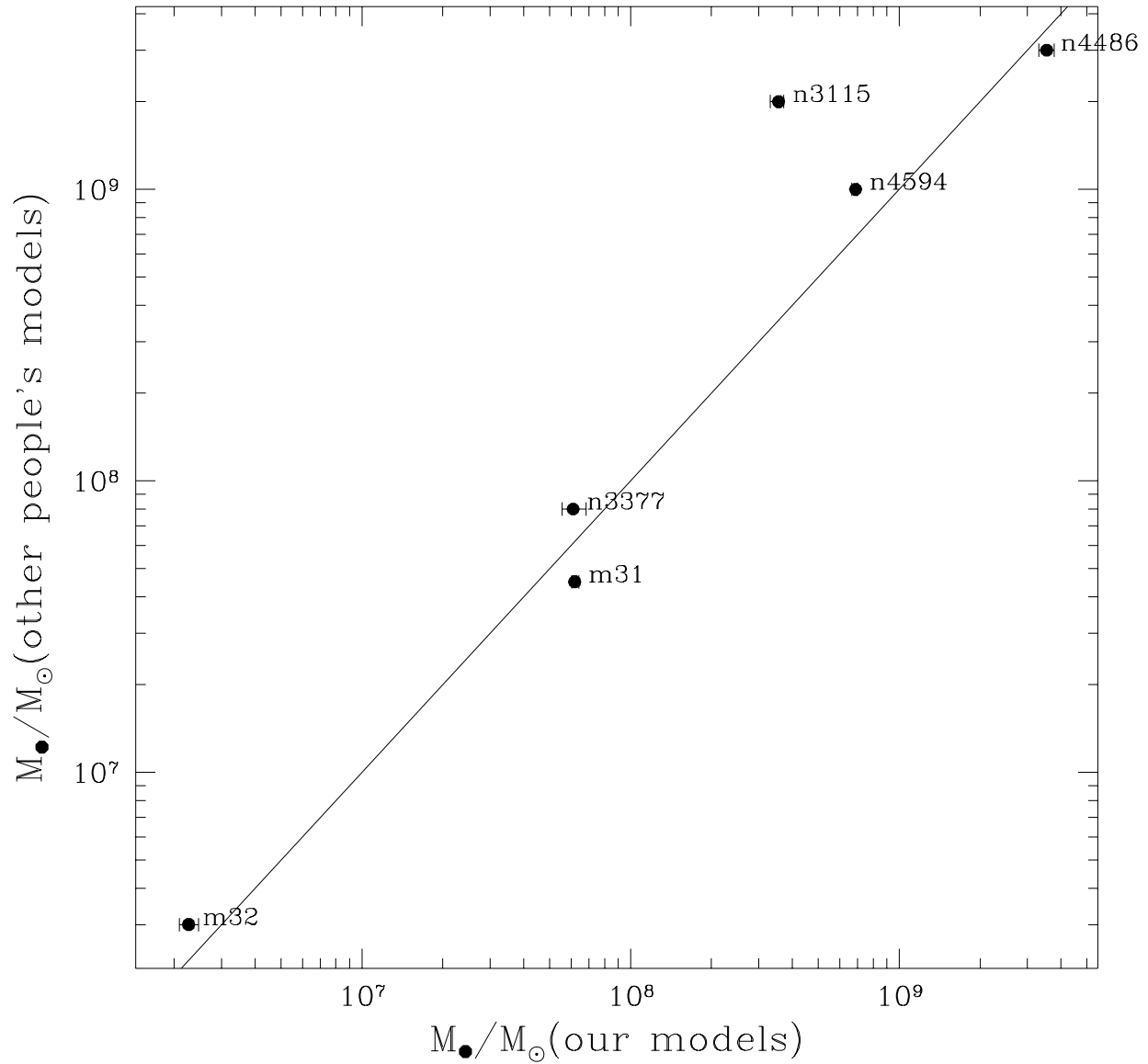


Figure 4. The correlation between the MDO masses predicted by our models and those predicted by other methods. The errorbars give the 68% confidence limits on M_{\bullet} . Sources for the other models are as follows: M31 – Richstone et al. (1990); M32 – van der Marel et al. (1997); NGC 3377 – Richstone et al. (1997); NGC 3115 – Kormendy et al. (1996a); NGC 4594 – Kormendy et al. (1996b); NGC 4486 – Harms et al. (1994).

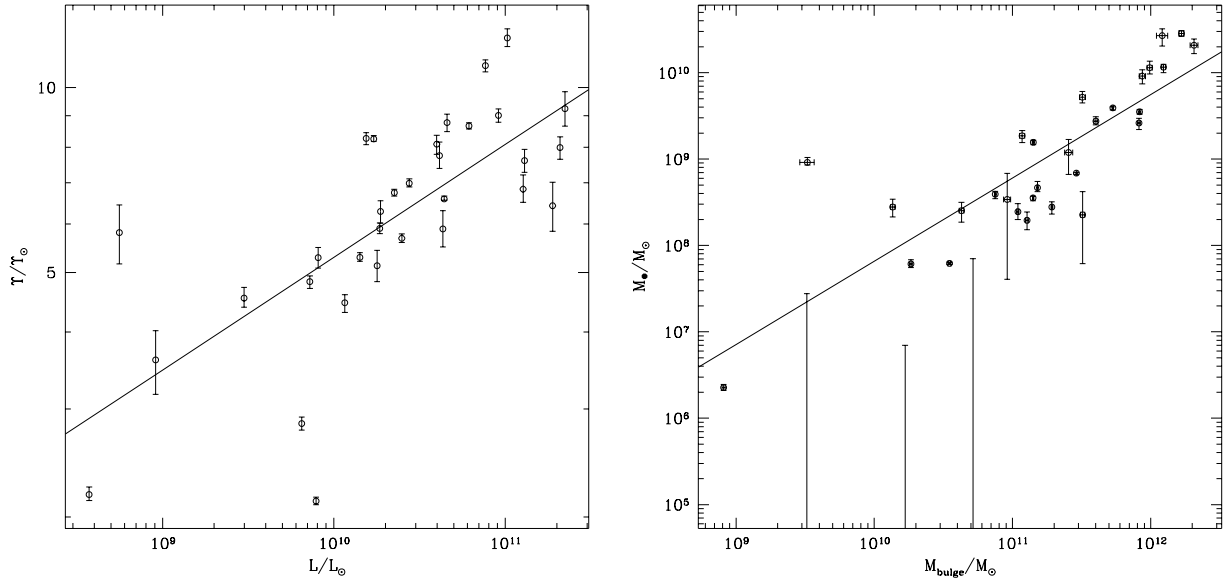


Figure 5(a) and (b). The correlations between stellar mass-to-light ratio Υ and bulge luminosity L (left panel) and between MDO mass M_{\bullet} and M_{bulge} (right panel) produced by our models. The error bars give 68% confidence intervals. The solid lines plot Υ_{fit} and $M_{\bullet,\text{fit}}$ as described in the text (equations (9) and (10)).

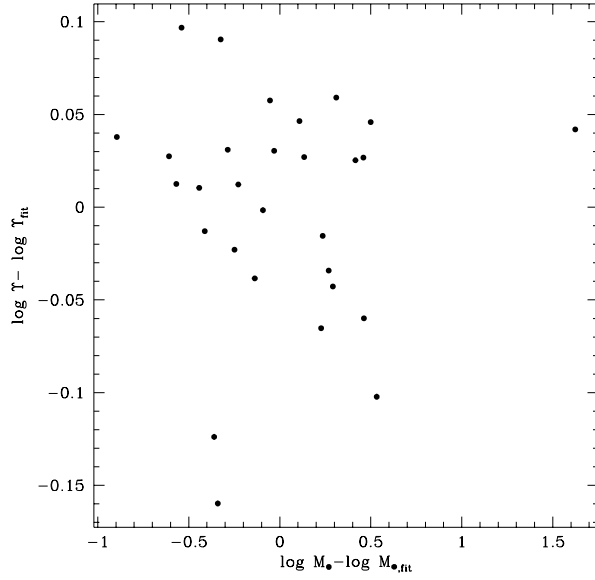


Figure 5(c). The correlation of the residuals in the Υ -versus- L and M_{\bullet} -versus- M_{bulge} fits.

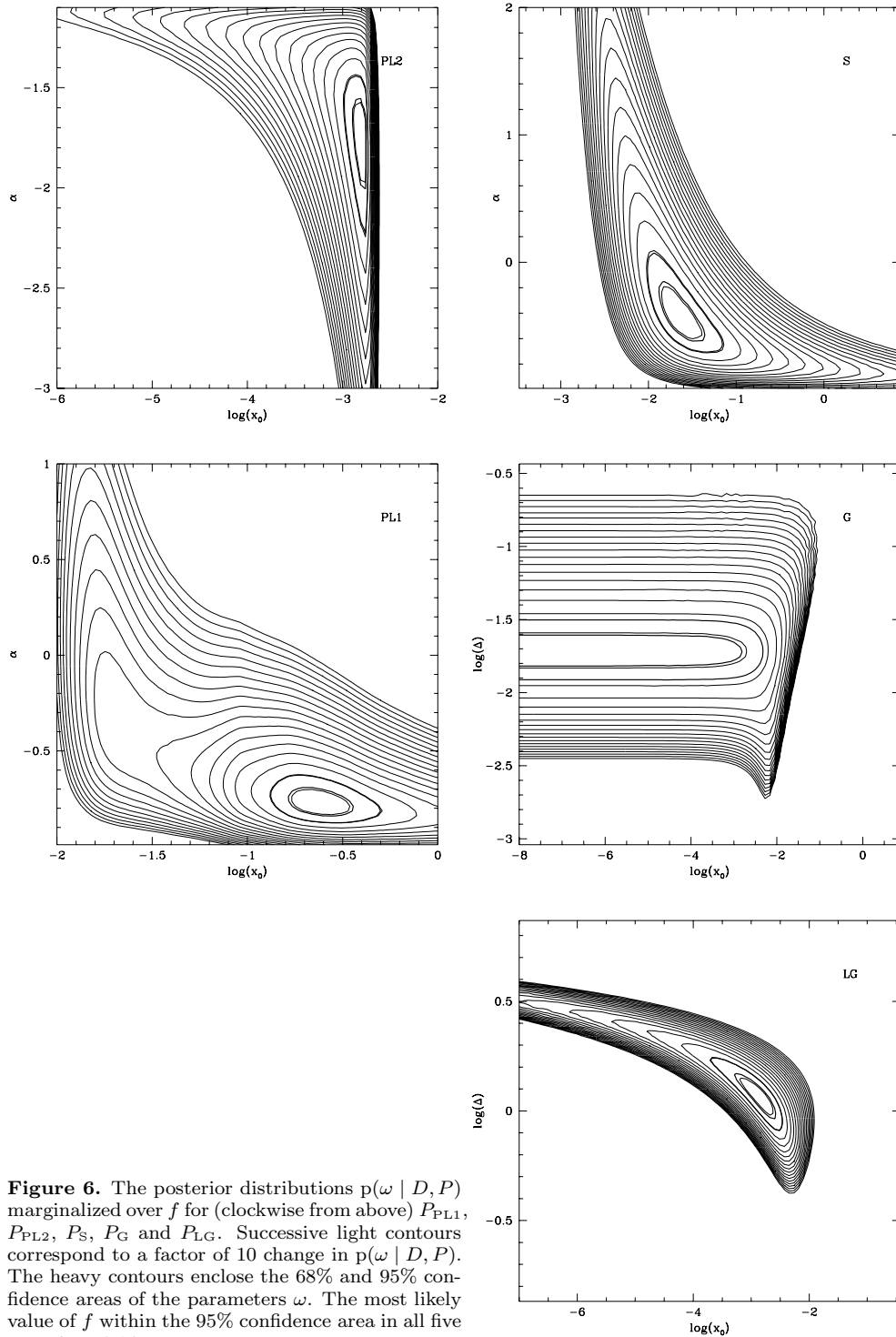


Figure 6. The posterior distributions $p(\omega \mid D, P)$ marginalized over f for (clockwise from above) P_{PL1} , P_{PL2} , P_{S} , P_{G} and P_{LG} . Successive light contours correspond to a factor of 10 change in $p(\omega \mid D, P)$. The heavy contours enclose the 68% and 95% confidence areas of the parameters ω . The most likely value of f within the 95% confidence area in all five cases is ~ 0.96 .

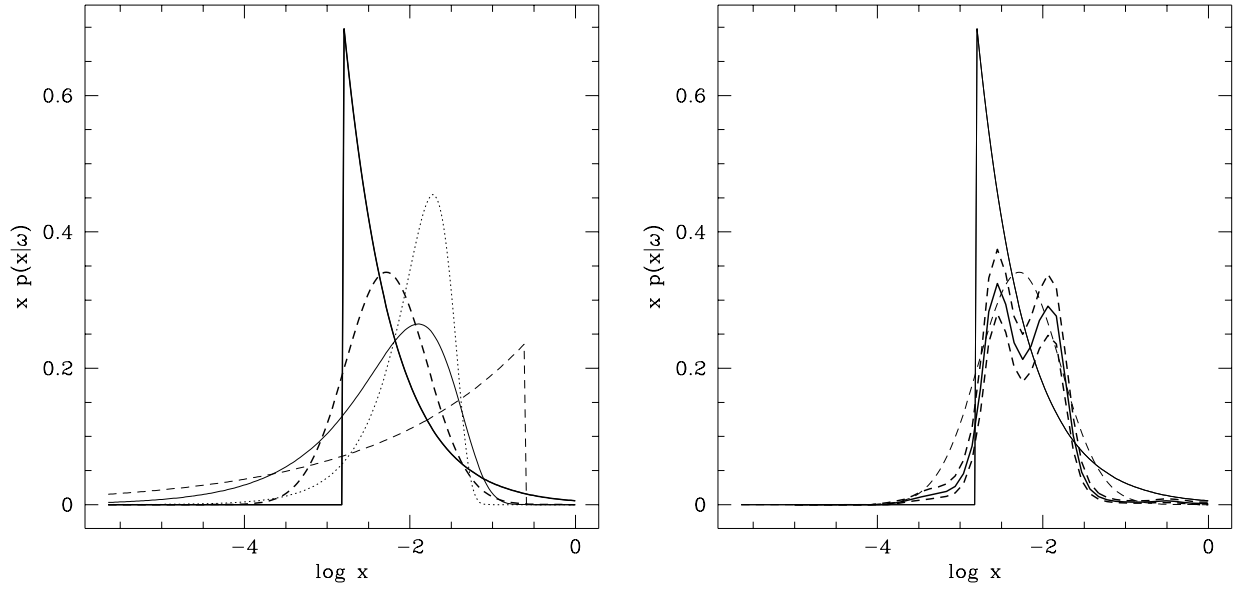


Figure 7(a). (Left panel) The probability distributions $p(x | \omega, P)$ for the best-fitting parameters ω . The heavy solid and dashed curves show results for P_{PL2} and P_{LG} , the two best-fitting cases. The lighter solid, dashed and dotted curves are for P_S , P_{PL1} and P_G respectively. (b). (Right panel) The “non-parametric” probability distribution $p(x)$ (heavy solid curve) and its 68% confidence limits (heavy dashed curves) obtained using the Metropolis algorithm with $\lambda = 5$. The rise in $p(x)$ at small x is caused by those galaxies without an MDO. The best-fitting parameterized distributions P_{PL2} and P_{LG} are overlaid as the lighter solid and dashed curves respectively.

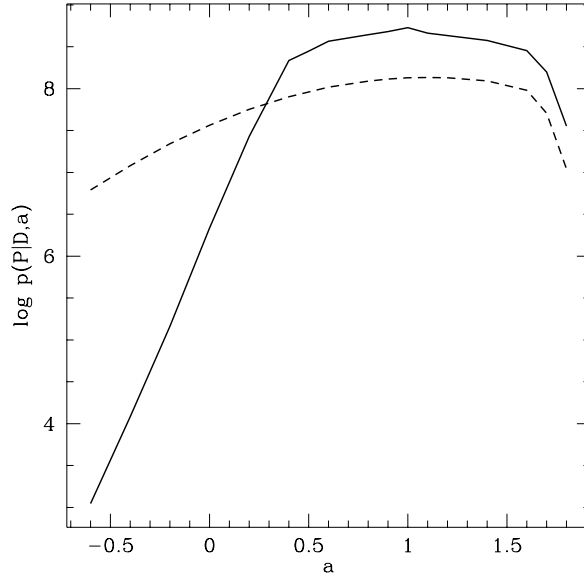


Figure 8. Variation of $p(P | D, a)$ with a , where a is defined in equation (18). The solid and dashed curves show $P = P_{PL2}$ and $P = P_{LG}$ respectively. The vertical scale does not extend down far enough to show the results for the other three parameterizations.

| Galaxy | type | M_V | R_{\min} (arcsec) | Outer Photometry | Slit pos ^a | seeing (arcsec) | max. radius (arcsec) | no. of bins | Kin. Source |
|--------|----------------|--------|------------------------|----------------------------|--------------------------|--------------------|-------------------------|----------------|----------------|
| | (1) | (2) | (3) | (4) | (5) | (6) | (7) | (8) | (9) |
| m31 | S \cap | -19.82 | - | Ke87 | maj. (bulge) | 0.6 | 8.9 | 34 | KB97 |
| | | | | | maj. (bulge) | 0.75 | 8.2 | 18 | vdM94b |
| | | | | | min. (bulge) | 1.2 | 8.3 | 17 | vdM94b |
| | | | | | maj. (nucl.) | 1.16 | 10 | 19 | vdM94b |
| | | | | | min. (nucl.) | 0.75 | 8.3 | 17 | vdM94b |
| m32 | E \setminus | -16.60 | - | L92b | maj. | 0.52 | 4 | 16 | BKD |
| | | | | | maj. | 0.75 | 7.5 | 13 | vdM94b |
| | | | | | min. | 0.83 | 11.3 | 9 | vdM94b |
| | | | | | 45° diag | 0.83 | 12 | 18 | vdM94b |
| n821 | E \setminus | -20.64 | - | BDM | maj. | 2.0 | 11.3 | 8 | BSG |
| | | | | | maj. | 2.0 | 27.5 | 24 | G93 |
| | | | | | min. | 2.0 | 17.5 | 16 | G93 |
| n1399 | E \cap | -21.71 | - | FIH | maj. | 2.0 | 37.3 | 12 | FIH |
| | | | | | min. | 2.0 | 38.5 | 12 | FIH |
| n1600 | E \cap | -22.70 | - | BDM | maj. | 2.0 | 24.9 | 23 | JS |
| | | | | | maj. | 2.0 | 27 | 22 | G93 |
| | | | | | min. | 2.0 | 18.4 | 18 | JS |
| | | | | | min. | 2.0 | 18.5 | 16 | G93 |
| n1700 | E \setminus | -21.65 | - | FIH | maj. | 2.0 | 23.8 | 8 | BSG |
| | | | | | maj. | 2.0 | 20 | 11 | FIH |
| | | | | | min. | 2.0 | 20.5 | 7 | BSG |
| | | | | | min. | 2.0 | 19.6 | 11 | FIH |
| n2300 | E \cap | -21.82 | - | BDM | maj. | 2.0 | 15.2 | 8 | BSG |
| | | | | | maj. | 2.0 | 21.5 | 18 | G93 |
| | | | | | min. | 2.0 | 29.6 | 8 | BSG |
| | | | | | min. | 2.0 | 20 | 19 | G93 |
| n2778 | E \setminus | -20.33 | - | PDIDC | maj. | 2.0 | 5.5 | 7 | FIF95 |
| | | | | | maj. | 2.0 | 11.5 | 10 | G93 |
| | | | | | min. | 2.0 | 3.9 | 9 | JS |
| | | | | | min. | 2.0 | 10 | 10 | G93 |
| n2832 | E \cap | -22.95 | - | PDIDC | maj. | 2.0 | 25.6 | 13 | FIF95 |
| n3115 | S0 \setminus | -20.75 | - | BDM | maj. | 0.57 | 43.8 | 56 | K96a |
| | | | | | maj. | 2.0 | 21.2 | 56 | BSG |
| | | | | | maj. | 1.0 | 30.7 | 25 | KR92 |
| | | | | | maj. | 1.0 | 28.4 | 20 | KR92 |
| | | | | | maj. | 1.0 | 24.7 | 23 | KR92 |
| | | | | | min. | 1.0 | 6.7 | 10 | KR92 |
| n3377 | E \setminus | -19.70 | - | SB | maj. | 0.59 | 22.6 | 30 | K97b |
| | | | | | maj. | 0.47 | 1.5 | 18 | K97b |
| | | | | | min. | 2.0 | 28.5 | 26 | G93 |
| n3379 | E \cap | -20.55 | - | PDIDC | maj. | 1.5 | 11.5 | 9 | G97 |
| | | | | | 18° diag. | 1.5 | 11.5 | 8 | G97 |
| | | | | | 28° diag. | 1.5 | 11.6 | 8 | G97 |
| | | | | | 72° diag. | 1.5 | 11.5 | 8 | G97 |
| n3608 | E \cap | -20.84 | - | BDM | maj. | 2.0 | 37.3 | 21 | JS |
| | | | | | maj. | 2.0 | 24.5 | 20 | G93 |
| | | | | | min. | 2.0 | 25.9 | 17 | JS |
| | | | | | min. | 2.0 | 24 | 19 | G93 |
| n4168 | E \cap | -21.76 | - | BDM | maj. | 2.0 | 30.6 | 11 | BSG |
| | | | | | maj. | 1.5 | 7.8 | 6 | BN |
| n4278 | E \cap | -21.16 | 0.1 | PDIDC | maj. | 2.0 | 31 | 36 | G93 |
| | | | | | min. | 2.0 | 30 | 30 | G93 |
| n4291 | E \cap | -20.85 | - | BDM | maj. | 2.0 | 28 | 21 | JS |
| | | | | | maj. | 2.0 | 19.5 | 13 | BSG |
| | | | | | min. | 2.0 | 24.1 | 17 | JS |
| | | | | | min. | 2.0 | 16.5 | 12 | BSG |
| n4365 | E \cap | -22.06 | - | $R_{\text{eff}} = 57''(1)$ | maj. | 2.0 | 7.5 | 7 | BSG |
| | | | | | min. | 2.0 | 6.3 | 6 | BSG |

| | | | | | | | | | |
|---------------|----------|--------|-----|----------------------------|-----------|------|------|----|--------|
| n4467 | E\ | -17.04 | - | $R_{\text{eff}} = 10''(f)$ | maj. | 1.5 | 7.5 | 6 | BN |
| n4472 | E \cap | -22.57 | - | PDIDC | maj. | 2.0 | 23.9 | 18 | BSG |
| | | | | | min. | 2.0 | 27.9 | 14 | BSG |
| n4473 | E \cap | -20.80 | - | BDM | maj. | 2.0 | 20.4 | 11 | BSG |
| n4486 | E \cap | -22.38 | - | PDIDC | maj. | 0.79 | 5.8 | 27 | vdM94a |
| n4486b | E \cap | -17.57 | - | $R_{\text{eff}} = 1''(f)$ | maj. | 0.66 | 5.5 | 15 | K97a |
| | | | | | maj. | 0.52 | 1.1 | 11 | K97a |
| | | | | | min. | 2.0 | 7.4 | 5 | BN |
| n4494 | E\ | -21.14 | - | BDM | maj. | 2.0 | 32.3 | 14 | BSG |
| | | | | | min. | 2.0 | 36.8 | 20 | JS |
| n4552 | E \cap | -21.05 | 0.1 | BDM | maj. | 3.0 | 24.9 | 8 | BSG |
| | | | | | maj. | 3.0 | 34.5 | 42 | G93 |
| | | | | | min. | 3.0 | 33.5 | 36 | G93 |
| n4564 | E\ | -19.94 | - | BDM | maj. | 2.0 | 33.2 | 16 | BSG |
| n4589 | E \cap | -21.69 | - | $R_{\text{eff}} = 30''(f)$ | maj. | 2.0 | 8.1 | 5 | BSG |
| n4594 | S0\ | -21.78 | 0.1 | K88 | maj. | 0.93 | 4.7 | 19 | K88 |
| | | | | | maj. | 0.93 | 4.9 | 11 | K88 |
| | | | | | maj. | 0.93 | 5 | 15 | vdM94b |
| | | | | | maj. | 0.93 | 4.2 | 7 | vdM94b |
| | | | | | min. | 0.93 | 8.2 | 10 | K88 |
| n4621 | E\ | -21.27 | - | BDM | maj. | 2.0 | 33.6 | 19 | BSG |
| | | | | | min. | 2.0 | 27.1 | 16 | BSG |
| n4636 | E \cap | -21.67 | - | BDM | maj. | 3.0 | 33.5 | 15 | BSG |
| n4649 | E \cap | -22.14 | - | BDM | maj. | 2.0 | 24.2 | 13 | BSG |
| | | | | | maj. | 2.0 | 37.5 | 35 | G93 |
| | | | | | min. | 2.0 | 27.7 | 16 | BSG |
| | | | | | min. | 2.0 | 34.5 | 52 | G93 |
| n4660 | E\ | -18.86 | - | SB | maj. | 2.0 | 8.1 | 8 | BSG |
| | | | | | min. | 2.0 | 5.5 | 6 | BSG |
| n4874 | E \cap | -23.54 | - | PDIDC | 26° diag. | 2.0 | 22.5 | 10 | FIF95 |
| n4889 | E \cap | -23.36 | - | BDM | maj. | 2.0 | 21.3 | 11 | FIF95 |
| n6166 | E \cap | -23.47 | 0.2 | $R_{\text{eff}} = 56''(l)$ | maj. | 2.0 | 12.9 | 13 | FIF95 |
| | | | | | min. | 2.0 | 5.5 | 9 | FIF95 |
| n7332 | S0\ | -19.91 | - | FIF94 | maj. | 2.0 | 31.3 | 33 | FIF94 |
| | | | | | maj. | 2.0 | 41.7 | 41 | FIF94 |
| | | | | | min. | 2.0 | 9.9 | 16 | FIF94 |
| | | | | | 45° diag. | 2.0 | 19.6 | 33 | FIF94 |
| | | | | | min.+6" | 2.0 | 12.5 | 10 | FIF94 |
| | | | | | maj.+6" | 2.0 | 14.1 | 14 | FIF94 |
| n7768 | E \cap | -22.93 | 0.4 | $R_{\text{eff}} = 30''(l)$ | maj. | 2.0 | 5.5 | 10 | FIF95 |
| | | | | | min. | 2.0 | 4.8 | 6 | FIF95 |

Table 1. The galaxy sample. Column (1) gives the galaxy type: “S”=spiral bulge, “S0”=lenticular, “E”=elliptical; “ \cap ”=cored, “\”=power law (Lauer et al. 1995). The absolute V magnitudes of the bulge or other hot component in column (2) are taken from Faber et al. (1997), and assume $H_0 = 80 \text{ km s}^{-1} \text{ Mpc}^{-1}$. R_{min} in column (3) is the radius inside which we believe the galaxy light may be contaminated by non-stellar radiation. Column (4) gives the source of the outer photometry used (if available), otherwise it gives the effective radius R_{eff} used for the outward extrapolation. Values of R_{eff} obtained from the literature are followed by an '(l)', while an '(f)' follows those obtained by fitting to the HST photometry. Columns (5) to (9) list the kinematical data used. For each exposure along each slit position, columns (5) and (6) give the position and FWHM of the seeing respectively. The maximum radius and the number of bins used by our models are given in columns (7) and (8). Finally, column (9) gives the source of the kinematical data.

| Galaxy | D/Mpc | $\log(L/L_\odot)$ | $\log(\Upsilon/\Upsilon_\odot)$ | $\log(M_\bullet/M_\odot)$ | $\log x$ |
|--------|----------------|-------------------|---------------------------------|----------------------------|----------------------------|
| m31 | 0.8 | 9.860 | $0.684^{+0.010}_{-0.011}$ | $7.792^{+0.016}_{-0.011}$ | $-2.752^{+0.021}_{-0.017}$ |
| m32 | 0.8 | 8.572 | $0.338^{+0.012}_{-0.010}$ | $6.355^{+0.036}_{-0.034}$ | $-2.553^{+0.040}_{-0.046}$ |
| n821 | 19.5 | 10.188 | $0.918^{+0.009}_{-0.011}$ | $8.291^{+0.097}_{-0.107}$ | $-2.796^{+0.085}_{-0.137}$ |
| n1399 | 17.9 | 10.616 | $0.889^{+0.022}_{-0.021}$ | $9.718^{+0.065}_{-0.068}$ | $-1.785^{+0.075}_{-0.091}$ |
| n1600 | 50.2 | 11.012 | $1.081^{+0.015}_{-0.014}$ | $10.065^{+0.033}_{-0.064}$ | $-2.046^{+0.060}_{-0.059}$ |
| n2300 | 31.8 | 10.660 | $0.943^{+0.014}_{-0.015}$ | $9.438^{+0.051}_{-0.043}$ | $-2.161^{+0.058}_{-0.060}$ |
| n2778 | 33.6 | 10.064 | $0.650^{+0.013}_{-0.016}$ | < 7.849 | < -2.850 |
| n2832 | 90.2 | 11.112 | $0.881^{+0.018}_{-0.019}$ | $10.058^{+0.076}_{-0.072}$ | $-1.935^{+0.089}_{-0.091}$ |
| n3115 | 8.4 | 10.232 | $0.917^{+0.005}_{-0.004}$ | $8.551^{+0.019}_{-0.032}$ | $-2.602^{+0.025}_{-0.030}$ |
| n3377 | 9.9 | 9.812 | $0.453^{+0.010}_{-0.011}$ | $7.786^{+0.049}_{-0.041}$ | $-2.469^{+0.045}_{-0.060}$ |
| n3379 | 9.9 | 10.152 | $0.724^{+0.008}_{-0.006}$ | $8.595^{+0.031}_{-0.053}$ | $-2.284^{+0.037}_{-0.056}$ |
| n3608 | 20.3 | 10.268 | $0.771^{+0.009}_{-0.008}$ | $8.392^{+0.091}_{-0.091}$ | $-2.638^{+0.088}_{-0.108}$ |
| n4168 | 36.4 | 10.636 | $0.770^{+0.030}_{-0.030}$ | $9.077^{+0.151}_{-0.253}$ | $-2.356^{+0.194}_{-0.273}$ |
| n4278 | 17.5 | 10.396 | $0.755^{+0.007}_{-0.007}$ | $9.194^{+0.024}_{-0.027}$ | $-1.959^{+0.030}_{-0.032}$ |
| n4291 | 28.6 | 10.272 | $0.798^{+0.018}_{-0.019}$ | $9.271^{+0.060}_{-0.079}$ | $-1.807^{+0.081}_{-0.091}$ |
| n4467 | 15.3 | 8.748 | $0.764^{+0.045}_{-0.051}$ | < 7.442 | < -2.025 |
| n4472 | 15.3 | 10.960 | $0.955^{+0.010}_{-0.011}$ | $9.417^{+0.055}_{-0.074}$ | $-2.509^{+0.074}_{-0.072}$ |
| n4473 | 15.8 | 10.252 | $0.710^{+0.025}_{-0.026}$ | $8.533^{+0.301}_{-0.923}$ | $-2.456^{+0.329}_{-1.338}$ |
| n4486 | 15.3 | 10.884 | $1.036^{+0.009}_{-0.010}$ | $9.549^{+0.028}_{-0.029}$ | $-2.377^{+0.041}_{-0.031}$ |
| n4486b | 15.3 | 8.960 | $0.557^{+0.048}_{-0.056}$ | $8.963^{+0.055}_{-0.033}$ | $-0.541^{+0.083}_{-0.100}$ |
| n4552 | 15.3 | 10.352 | $0.829^{+0.006}_{-0.005}$ | $8.669^{+0.072}_{-0.045}$ | $-2.495^{+0.059}_{-0.068}$ |
| n4564 | 15.3 | 9.908 | $0.723^{+0.017}_{-0.017}$ | $8.404^{+0.097}_{-0.132}$ | $-2.240^{+0.118}_{-0.136}$ |
| n4594 | 9.2 | 10.644 | $0.819^{+0.005}_{-0.002}$ | $8.838^{+0.006}_{-0.015}$ | $-2.631^{+0.013}_{-0.012}$ |
| n4621 | 15.3 | 10.440 | $0.844^{+0.007}_{-0.006}$ | $8.445^{+0.061}_{-0.083}$ | $-2.842^{+0.066}_{-0.086}$ |
| n4636 | 15.3 | 10.600 | $0.908^{+0.014}_{-0.016}$ | $8.356^{+0.267}_{-0.566}$ | $-3.154^{+0.273}_{-0.652}$ |
| n4649 | 15.3 | 10.788 | $0.938^{+0.005}_{-0.005}$ | $9.594^{+0.011}_{-0.023}$ | $-2.143^{+0.024}_{-0.016}$ |
| n4660 | 15.3 | 9.476 | $0.657^{+0.017}_{-0.015}$ | $8.446^{+0.090}_{-0.115}$ | $-1.699^{+0.110}_{-0.120}$ |
| n4874 | 93.3 | 11.348 | $0.966^{+0.028}_{-0.028}$ | $10.319^{+0.071}_{-0.097}$ | $-2.000^{+0.093}_{-0.119}$ |
| n4889 | 93.3 | 11.276 | $0.808^{+0.038}_{-0.042}$ | $10.429^{+0.079}_{-0.119}$ | $-1.678^{+0.127}_{-0.140}$ |
| n6166 | 112.5 | 11.320 | $0.902^{+0.018}_{-0.019}$ | $10.454^{+0.034}_{-0.029}$ | $-1.767^{+0.048}_{-0.047}$ |
| n7332 | 20.3 | 9.896 | $0.327^{+0.006}_{-0.006}$ | < 6.845 | < -3.373 |
| n7768 | 103.1 | 11.104 | $0.835^{+0.023}_{-0.021}$ | $9.961^{+0.072}_{-0.089}$ | $-1.991^{+0.101}_{-0.103}$ |

Table 2. The best-fitting parameters (Υ , M_\bullet and $x \equiv M_\bullet/M_{\text{bulge}}$) with their 68% confidence intervals for the 32 galaxies that our models describe well. The assumed galaxy distance D and the luminosity L of the bulge or other hot stellar component are also listed.

| P | f | $\log x_0$ | α or $\log \Delta$ | $\log \langle x \rangle$ | $\langle \log x \rangle$ |
|------------------|---------------------------|----------------------------|----------------------------|----------------------------|----------------------------|
| P_{PL1} | $1.000^{+0.000}_{-0.057}$ | $-0.608^{+0.094}_{-0.125}$ | $-0.765^{+0.037}_{-0.056}$ | $-1.347^{+0.115}_{-0.111}$ | |
| P_{PL2} | $0.950^{+0.032}_{-0.065}$ | $-2.815^{+0.063}_{-0.038}$ | $-1.725^{+0.131}_{-0.161}$ | | $-2.266^{+0.097}_{-0.089}$ |
| P_{S} | $1.000^{+0.000}_{-0.067}$ | $-1.705^{+0.204}_{-0.109}$ | $-0.456^{+0.178}_{-0.112}$ | $-1.879^{+0.117}_{-0.107}$ | $-2.334^{+0.153}_{-0.187}$ |
| P_{G} | $0.940^{+0.042}_{-0.067}$ | $-4.747^{+0.222}_{-3.253}$ | $-1.717^{+0.098}_{-0.090}$ | $-1.809^{+0.106}_{-0.096}$ | $-1.993^{+0.106}_{-0.091}$ |
| P_{LG} | $0.970^{+0.030}_{-0.057}$ | $-2.842^{+0.206}_{-0.226}$ | $0.074^{+0.065}_{-0.065}$ | $-1.964^{+0.149}_{-0.119}$ | $-2.274^{+0.104}_{-0.111}$ |

Table 4. The best-fitting parameters ω and their 68% confidence limits for each assumed distribution $p(x | \omega, P)$. By definition $0 \leq f \leq 1$. The last two columns give the logarithm of the expectation value of $x \equiv M_{\bullet}/M_{\text{bulge}}$ and the expectation value of $\log x$ for those galaxies with $M_{\bullet} \neq 0$ (both calculated from $p_{+}(x | \omega, P)$). The mean $\langle x \rangle$ does not exist for P_{PL2} , while $\langle \log x \rangle$ does not exist for P_{PL1} .